

DYNAMICAL INTERACTION BETWEEN THE LOWER STRATOSPHERE AND THE TROPOSPHERE

TAKASHI NITTA*

National Meteorological Center, Weather Bureau, ESSA, Washington, D.C.

ABSTRACT

The vertical flux of geopotential and the conversion between eddy available potential and eddy kinetic energy due to non-stationary disturbances are studied by solving numerically the diagnostic as well as the prognostic equations of a linearized 20-level model. The vertical distribution of these quantities thus computed compares well with those obtained by other authors from observed data and also with the results of general circulation experiments.

The efforts of various parameters on these quantities are investigated by taking various experimental initial conditions for time integration of the prognostic equations. The parameters dealt with are: the scale of disturbance waves, the vertical tilt of the waves, the vertical profile of the zonal flow, the static stability, the β -effect, and viscosity. The results show that the vertical tilt of the ultra-long and the long waves is important for the time change of eddy kinetic energy near or above the tropopause, and that the tilt of the short wave is important in the lower troposphere. In all cases, the westward tilt with increasing altitude contributes to the increase in kinetic energy, and the eastward tilt contributes to the reverse. The vertical wind shear is influential in determining the vertical distribution of the quantities. The β -effect is important to the ultra-long wave in that the eddy kinetic energy is increased in the upper atmosphere because of its presence. Likewise, the eddy kinetic energy is suppressed in the lower troposphere. Viscosity affects mainly the short wave in the lower troposphere. The effect of the vertically integrated divergence on the westward displacement of the ultra-long wave is also discussed.

CONTENTS

1. Introduction.....	319
2. Consideration of the Dynamical Interaction.....	320
3. Linearized 20-Level Balanced Baroclinic Model.....	322
4. Results of Numerical Experiments.....	324
5. Discussion of the Results.....	332
6. Summary.....	335
Appendix:	
(A) A Simple Analytic Expression of Interacting Quantities.....	336
(B) Comparison of Numerical Solutions of the ω - Equation between Different Space Resolutions....	337
(C) Numerical Computation Procedure.....	337
(D) Exchange of Thermodynamical Units.....	338
Acknowledgments.....	338
References.....	338

1. INTRODUCTION

Recent studies of the energetics in the earth's atmosphere indicate that motions in the troposphere and lower stratosphere interact closely with each other in relation to eddy kinetic energy, to form a combined meteorological system. (Boville [4], Teweles [31], Reed, Wolfe, and Nishimoto [28], Miyakoda [18], Oort [25], Muench [19], [20], Julian and Labitzke [13], Smagorinsky, Manabe, and Holloway [29], Miller [17], Kung [15])

Eliassen and Palm [11] discussed (among other things) vertical transfer of energy in stationary geostrophic mountain waves throughout the atmosphere and obtained a relation between wave energy flux and meridional eddy flux of sensible heat for quasi-geostrophic motion. They showed the condition that limits the vertical penetration of wave energy. Charney and Drazin [6] and Charney and Pedlosky [7] treated the problem for stable and unstable

*On leave of absence from Japan Meteorological Agency, Tokyo, Japan.

waves. They looked for the condition of the existence of internal waves throughout the whole atmosphere, considering the existence of the waves as a prerequisite for vertical propagation of wave energy from the troposphere. They investigated the possibility of the penetration from functional forms of the governing equations for various sets of basic physical parameters. The criterion they obtained for the free vertical propagation of perturbation energy shows a high possibility of the trapping of waves around the tropopause or at a level in the lower stratosphere. Chen [8] dealt with the same problem as Charney and Drazin [6], but used a more general form of the governing equations to obtain similar results. Staff Members of Academia Sinica [30] studied a correlation of the stratospheric and tropospheric motions from the synoptic point of view. They found a close relationship between both motions and emphasized the important role played by the very long waves. The Chinese group also examined their results theoretically with simple models. Dickinson [10] treated the propagation problem of the atmospheric waves comprehensively and extensively from the theoretical point of view.

All the authors mentioned above obtained their conclusions from examining the functional form of the governing equations and/or dealing with special analytical solutions, without solving the governing equations directly with respect to time. On the other hand, Onishi and Tanabe [24] pursued numerically with respect to time the vertical propagation of wave energy from a source, using a simple model. Recently, Murakami [21] performed a comprehensive numerical estimate of the vertical redistribution of energy due to stationary waves induced by topography and diabatic heat sources and sinks. He showed the relation between the characteristics of the vertical redistribution of energy and the scale of the stationary waves.

Numerical simulation of the general circulation of the atmosphere provided us the more general information about the dynamical coupling between the lower stratosphere and the troposphere in terms of energetics. (See for example, Smagorinsky, Manabe, and Holloway [29].)

Numerical analysis of observations by Kung [15] indicates daily variations and a seasonal march of the energetic interplay between the lower stratosphere and the troposphere. The calculation with the real data by Nitta [23] also shows frequent daily changes of the vertical flux of geopotential through the tropopause.

According to investigations thus far, it would be generally accepted that eddy kinetic energy which is converted in the troposphere from eddy available potential energy is redistributed upward into the lower stratosphere. For actual performance, the vertical distribution of zonal mean flow and that of zonal mean static stability, the inclination of the wave axis, and the scale of disturbance may be involved. The above-mentioned studies more or less focus their attention on the interrelation between wave patterns or on the vertical redistribution of eddy energy between atmospheric layers

It seems to the present author that there are few completely general works with the non-linear equations which treat the energetic coupling from the viewpoint of the structure of non-stationary disturbances. Therefore, in the present paper a study on the large-scale kinetic energy budget throughout the lower stratosphere and the troposphere is treated in relation to the vertical structure of the baroclinic waves in the middle-latitude westerlies. The following interacting quantities are adopted here: the convergence of the vertical flux of geopotential, the conversion between the eddy available potential and the eddy kinetic energy, a sum of the two terms, and the vertical flux of geopotential. The probably important interaction through small-scale turbulent motions is not dealt with.

A linearized 20-level balanced baroclinic model is adopted. At first, the model is treated for a diagnostic study to obtain information on the vertical profiles of the interacting quantities for various combinations of physical parameters. Secondly, a numerical time integration is made with the computational model for 24 hr. from a specific initial condition where no energetic interaction occurs. There is no computational reason why the forecast is stopped just 24 hr. later, but it is felt that a 24-hr. period should be sufficient to gain insight into the aspects of the dynamic interaction.

To make up the numerical experiment, analytical methods could be used. However, determination of the eigenvalues for the governing equations is a very complicated procedure, especially for a multi-level model, even if we assume a simple vertical wind shear and a crude vertical profile of the zonal mean static stability. Also, we cannot specify the relation between an actual unified movement of a meteorological wave in a stratified atmosphere and its associated eigenvalues. Therefore, in the present paper a monochromatic sinusoidal wave is assumed as a disturbance, a priori. According to this wave pattern, analytical expressions of the interacting quantities are obtained based on an ω -equation in a simplified quasi-geostrophic system.

The present paper consists of the following sections: Section 2 considers the physical meaning of the dynamical interaction. Section 3 describes the computational model used for the numerical experiment. Section 4 presents results of the experiment. Section 5 discusses the results. The vertical distributions of the space-mean interacting quantities in the present experiment are compared with the results obtained with the general circulation model of Smagorinsky, Manabe, and Holloway [29] and with those of the numerical analysis of observed data by Kung [15]. The results obtained from the simple analytical solution are shown in Appendix A.

2. CONSIDERATION OF THE DYNAMICAL INTERACTION

The kinetic energy and available potential energy, K and A , in x (east), y (north), p (pressure) coordinates may

be defined, respectively, as

$$K = \frac{1}{2} (u^2 + v^2) \tag{2.1}$$

and

$$A = \frac{1}{2} B (T^*)^2 \tag{2.2}$$

where u and v are the horizontal components of velocity, T^* the deviation of temperature on an isobaric surface from its space mean, i.e.,

$$(\)^* = (\) - (\)^H, (\)^H = \iint (\) dx dy / \iint dx dy,$$

and

$$B = -\frac{R}{\frac{\partial \theta}{\partial p}} \frac{1}{p} \left(\frac{P}{p} \right)^{\epsilon} \tag{2.3}$$

where R is the gas constant, θ the potential temperature, and P the base pressure, 1000 mb. (See, for example, Miyakoda [18], Smagorinsky, Manabe, and Holloway [29].) The equations for the rate of change of the kinetic energy and available potential energy can be written without viscosity terms as

$$\begin{aligned} \frac{\partial K}{\partial t} = & - \left[\frac{\partial}{\partial x} (uK) + \frac{\partial}{\partial y} (vK) + \frac{\partial}{\partial p} (\omega K) \right] \\ & - \left[\frac{\partial}{\partial x} (u\phi) + \frac{\partial}{\partial y} (v\phi) + \frac{\partial}{\partial p} (\omega\phi) + \omega\alpha \right] \end{aligned} \tag{2.4}$$

and

$$\frac{\partial A}{\partial t} = - \left[\frac{\partial}{\partial x} (uA) + \frac{\partial}{\partial y} (vA) + \frac{\partial}{\partial p} (\omega A) \right] + \omega\alpha \tag{2.5}$$

where ϕ is the geopotential, α the specific volume. The two-dimensional space integral of equations (2.4) and (2.5) over the energetically closed domain turns out to be

$$\frac{\partial \overline{K}}{\partial t} = - \frac{\partial}{\partial p} (\overline{\omega K}) - \frac{\partial}{\partial p} (\overline{\omega\phi}) - \overline{\omega\alpha}^H \tag{2.6}$$

and

$$\frac{\partial \overline{A}}{\partial t} = - \frac{\partial}{\partial p} (\overline{\omega A}) + \overline{\omega\alpha}^H. \tag{2.7}$$

The first term on the right-hand side of equation (2.6) shows the rate of the vertical transport of kinetic energy, the second term a part of the pressure interaction or the convergence of the vertical flux of geopotential, and the third the energy conversion between the available potential energy and the kinetic energy. The first term on the right-hand side of equation (2.7) indicates the rate of the vertical transport of available potential energy, and the second term is the counterpart of the conversion in equation (2.6).

When we separate equations (2.6) and (2.7) into the part of the eddy energy and that of the zonal mean energy, we have

$$\frac{\partial \overline{K}'}{\partial t} = - \frac{\partial}{\partial p} (\overline{\omega K}') - \frac{\partial}{\partial p} (\overline{\omega' \phi'}) - \overline{\omega' \alpha'}^H + C(\overline{K}, K')^H \tag{2.8}$$

$$\frac{\partial \overline{K}}{\partial t} = - \frac{\partial}{\partial p} (\overline{\omega \overline{K}}) - \frac{\partial}{\partial p} (\overline{\omega \phi}) - \overline{\omega \alpha}^H - C(\overline{K}, K')^H \tag{2.9}$$

$$\frac{\partial \overline{A}'}{\partial t} = - \frac{\partial}{\partial p} (\overline{\omega A}') - \overline{\omega' \alpha'}^H + C(\overline{A}, A')^H \tag{2.10}$$

and

$$\frac{\partial \overline{A}}{\partial t} = - \frac{\partial}{\partial p} (\overline{\omega \overline{A}}) + \overline{\omega \alpha}^H - C(A, A')^H \tag{2.11}$$

where $\overline{(\)} = \int (\) dx / \int dx$, $(\)' = (\) - \overline{(\)}$, $K' = \frac{1}{2} (u'^2 + v'^2)$,

$\overline{K} = \frac{1}{2} (\overline{u^2} + \overline{v^2})$, $\overline{A} = \frac{1}{2} B (\overline{T^*})^2$, and $A' = A - \overline{A}$.

The terms $C(\overline{K}, K')^H$ and $C(\overline{A}, A')^H$ show the horizontal average of the rate of the conversion of zonal mean flow kinetic energy into perturbation kinetic energy and that of zonal mean flow available potential energy into perturbation available potential energy.

Generally speaking, the term "dynamical interaction between atmospheric layers" due to disturbances may be interpreted as the contribution to the local time change of the space mean total eddy energy, $\frac{\partial (A' + K')}{\partial t}^H$, at a layer from other layers by means of the space average convergence of the vertical flux of the quantities which relate to eddy energy, i.e., $-\frac{\partial (\overline{\omega K'})}{\partial p}^H$, $-\frac{\partial (\overline{\omega' \phi'})}{\partial p}^H$, and $-\frac{\partial (\overline{\omega A'})}{\partial p}^H$. Physical meaning of these terms is as follows: the first term means the vertical transport of eddy kinetic energy, the second term indicates a part of the contribution due to the pressure interaction in the vertical, and the third is the vertical transport of eddy available potential energy.

In the present paper, referring to the observed energetics in the lower stratosphere, we focus on the exchange of the eddy kinetic energy between the lower stratosphere and the troposphere through the tropopause. In this sense the two terms, $-\frac{\partial (\overline{\omega K'})}{\partial p}^H$ and $-\frac{\partial (\overline{\omega' \phi'})}{\partial p}^H$, will be considered. According to the results of the analysis of the real atmosphere (Miyakoda [18], Muench [19], [20], Oort [25], Miller [17], Kung [15], [16]), $-\frac{\partial (\overline{\omega K'})}{\partial p}^H$ is much smaller than $-\frac{\partial (\overline{\omega' \phi'})}{\partial p}^H$. Therefore, the former term will be ignored. As has already been pointed out by several authors (see Muench [20], Kung [15], etc.), the term $-\frac{\partial (\overline{\omega' \phi'})}{\partial p}^H$ is derived as a part of the term

$-\overline{\mathbf{V}' \cdot \nabla \phi'}^H$. The term $-\overline{\mathbf{V}' \cdot \nabla \phi'}^H$ means the contribution to the local time change of the eddy kinetic energy from the work done by the pressure force. When the term $-\overline{\partial(\omega' \phi')/\partial p}^H$ is integrated in the vertical from the top (where $\omega=0$ is assumed) to the bottom of the atmosphere, there remains $\overline{\omega' \phi'}^H$ at the ground surface, which is very small in magnitude. In this sense, the term $-\overline{\partial(\omega' \phi')/\partial p}^H$ may be called the redistribution term of the eddy kinetic energy. Another part derived from the term $-\overline{\mathbf{V}' \cdot \nabla \phi'}^H$ is the rate of the conversion between the eddy kinetic energy and the eddy available potential energy, i.e., $-\overline{\omega' \alpha'}^H$.

According to the analysis of observed data, the net increase in eddy kinetic energy for the whole atmosphere in middle latitudes is mainly due to the conversion term. The levels where the eddy kinetic energy is converted from the eddy available potential energy are located in the mid-troposphere. However, because of the redistribution term, levels where the net increase in the eddy kinetic energy results are located near or above the tropopause. In this way the lower stratosphere and the troposphere interact with each other energetically. Therefore, in the discussion to follow the vertical profiles of the terms, $-\overline{\partial(\omega' \phi')/\partial p}^H$, $-\overline{\omega' \alpha'}^H$, and the sum of the two terms $-\overline{\mathbf{V}' \cdot \nabla \phi'}^H$ will be examined in relation to the structure of waves. Throughout the following discussion, the interacting quantities are designated as follows:

- (1) the redistribution term, $-\overline{\partial(\omega' \phi')/\partial p}^H$,
- (2) the conversion term, $-\overline{\omega' \alpha'}^H$,
- (3) the generation term, $-\overline{\mathbf{V}' \cdot \nabla \phi'}^H = -\overline{\frac{\partial}{\partial p}(\omega' \phi')}^H - \overline{\omega' \alpha'}^H$.

The energy equations which are derived from prognostic equations adopted in the numerical experiment do not agree with equations (2.4) and (2.5). The discrepancy, however, may be negligibly small, and hereafter the energetics will be considered in reference to equations (2.4) through (2.11). It should also be noted that the total energy is not conserved in the linearized forecast model which will be described in the next section, because it is assumed that the zonal mean flow and its vertical shear are constant with time. This means that the eddy available potential energy is always supplied from the zonal mean available potential energy, i.e., $\overline{C(\bar{A}, A')}^H > 0$.

3. LINEARIZED 20-LEVEL BALANCED BAROCLINIC MODEL

BASIC ASSUMPTIONS

In this simplified model research, we adopt the following principal assumptions.

(1) For the sake of simplicity, the β -plane approximation is used. According to the usual scale theory, the characteristic horizontal scale of the very long waves is comparable to the earth's radius and the β -plane assumption is no longer valid (Burger [5], Phillips [27]). The spectral analysis of observed data, however, shows that the horizontal scale of the very long waves in the meridional direction seems to be much smaller than that in the zonal direction (Eliassen [12], Phillips [27]). Although abandonment of spherical treatment might bring errors and we should eventually deal with the problem in three-dimensional spherical space, the present application of the β -plane approximation for the very long waves seems to be not a fatal fault. (See Welander [32].)

(2) Motion is confined in the x, p plane and the governing equations are linearized. The zonal mean velocity, $U(p)$, is assumed to be constant for all time.

(3) Meridional variation of physical quantities concerning the disturbance is ignored and those of the zonal mean height and temperature are expressed so as to satisfy the geostrophic and thermal wind relations, respectively. Therefore, this system is not energetically closed. This assumption turns out to be the limitation of our prognostic model. Namely, if we pose a baroclinically unstable vertical wind shear for the zonal current, development of a wave will go on endlessly, because there is no feed-back to weaken the vertical wind shear.

(4) To examine the influence of dissipation, the following Austausch coefficient or gross viscosity is assumed:

(a) Rate of momentum and heat changes with respect to time due to the lateral diffusion, i.e.,

$$\mathbf{F}_v = \nu \nabla^2 \mathbf{V}$$

for the equations of motion, and

$$\mathbf{F}_T = \nu \nabla^2 T$$

for the thermal equation, where $\nu = 2 \times 10^5 \text{ m}^2 \text{ sec}^{-1}$ is used.

(b) Rate of momentum change with respect to time due to the vertical diffusion, i.e.,

$$\mathbf{F}_v^* = -g \frac{\partial \tau}{\partial p}$$

for the equations of motion, where g is the acceleration of gravity, and

$$\tau = -\rho^3 g^2 l^2 \left| \frac{\partial \mathbf{V}}{\partial p} \right| \cdot \frac{\partial \mathbf{V}}{\partial p} \text{ for } 800 \text{ mb.} \leq p < 1000 \text{ mb.},$$

$$\tau = \tau_s = \rho_s C_D |\mathbf{V}| \cdot \mathbf{V} \text{ for } p = 1000 \text{ mb.},$$

ρ is the density of air, ρ_s is that at the ground surface, l the mixing length which is prescribed as $l=0$ (for 800 mb.), $l=12$ m. (for 850 mb.), $l=18$ m. (for 900 mb.), and $l=24$ m. (for 950 mb.), and C_D is the drag coefficient of numerical value 3×10^{-3} . (Concerning levels where τ is given, see the assumption (6).)

The experiment is performed with and without dissipation. Unless explicitly stated otherwise, the computation was performed without diffusion in both the lateral and vertical directions.

(5) Since our horizontal domain is limited to 12,000 km. in size, the maximum wavelength which we can deal with here is also 12,000 km. In the numerical experiment, the following three waves are adopted as the representatives of three characteristic wave components in the atmosphere, i.e.,

(i) a wave of wavelength 12,000 km. for representing the very long waves,

(ii) a wave of wavelength 6000 km. for representing the long waves, and

(iii) a wave of wavelength 3000 km. for representing the short waves.

(6) As is shown in figure 3.1, the domain is resolved in 20 layers in the vertical (pressure increment $\Delta p = 50$ mb.) and 60 grids in the horizontal (grid interval $d = 200$ km.). For a part of the diagnostic study, the area is meshed horizontally with 30 grids ($d = 400$ km.) for computational convenience. (See Appendix B.) In this connection, one hour is adopted as the time interval Δt . It is also assumed that the pressure at the tropopause is 200 mb. This means that there are four layers in the stratosphere and 16 layers in the troposphere. As the uppermost level where the height field is specified is 25 mb., it may be said that in the present model the lower stratosphere can approximately be taken into account.

(7) Concerning the lateral boundary condition, the cyclic continuity for all variables is assumed. Upper and lower boundary conditions are

$$\omega = 0 \text{ at } p = 0 \text{ mb.}, \quad (3.1)$$

and

$$\omega = \omega_s \text{ at } p = 1000 \text{ mb.}, \quad (3.2)$$

respectively, where ω_s is the vertical p -velocity at the lowest surface and will be specified later. (See section 4.)

NUMERICAL MODEL

Since we desire a comprehensive treatment of the large-scale atmospheric motions from the ultra-long waves to the short waves, the computational model should be a balanced baroclinic model in the broad sense or a primitive equation model. Therefore, the linearized 20-level balanced baroclinic model is designed and constructed here in the present experiment under the assumptions mentioned earlier. A similar model was used by Arakawa [3] to study non-geostrophic effects.

The governing equations are the vorticity equation:

$$\frac{\partial^2}{\partial x^2} \frac{\partial}{\partial t} Z'_k = -U_k \frac{\partial}{\partial x} \left(\frac{\partial^2}{\partial x^2} Z'_k \right) - \beta \frac{\partial}{\partial x} Z'_k + \frac{f_0^2}{g} \frac{\omega'_{k+1/2} - \omega'_{k-1/2}}{\Delta p} + \frac{f_0}{g} D_k \quad (3.3)$$

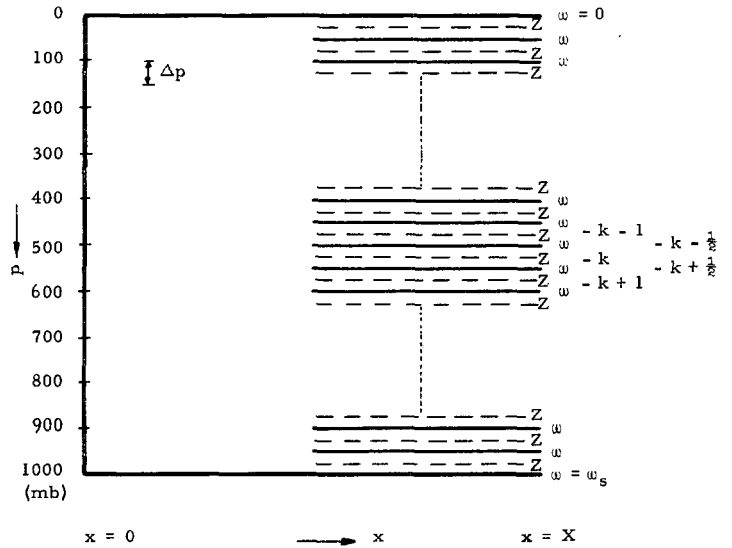


FIGURE 3.1.—Vertical resolution in x, p plane for the numerical model ($X=12,000$ km.).

the thermal equation:

$$\frac{\partial}{\partial t} (Z'_k - Z'_{k+1}) = -U_{Hk} \frac{\partial}{\partial x} h'_{k+1/2} - \frac{g}{f_0} \left(\frac{\partial}{\partial x} Z'_{k+1/2} \right) \left(\frac{\partial}{\partial y} \bar{h}_{k+1/2} \right) + \frac{\Delta p}{g} S_{k+1/2} \omega'_{k+1/2} + E_{k+1/2} \quad (3.4)$$

the ω -equation:

$$S_{k+1/2} \frac{\partial^2}{\partial x^2} \omega'_{k+1/2} + \frac{f_0^2}{\Delta p^2} (\omega'_{k+1/2} + \omega'_{k-1/2} - 2\omega'_{k+1/2}) = \frac{g}{\Delta p} (VAD_{k+1} - VAD_k) + \frac{g}{\Delta p} \frac{\partial^2}{\partial x^2} HAD_k + \frac{f_0}{\Delta p} (D_k - D_{k+1}) - \frac{g}{\Delta p} \frac{\partial^2}{\partial x^2} E_{k+1/2} \quad (3.5)$$

and the S -equation:

$$\frac{\partial}{\partial t} S_{k+1/2} = \frac{g}{\Delta p} \frac{1}{p^{(1/\gamma)}} \frac{1}{\Delta p^2} (PWH_{k+1/2} + PWH_{k-1/2} - 2 \cdot PWH_{k+1/2}) \quad (3.6)$$

where

$$\bar{h} = (\bar{Z}_k - \bar{Z}_{k+1})/l, \quad \gamma = c_p/c_v, \quad PWH_k = p^{1/\gamma} \omega' h' \quad (3.7)$$

$$VAD_k = U_k \frac{\partial}{\partial x} \left(\frac{\partial^2}{\partial x^2} Z'_k \right) + \beta \frac{\partial}{\partial x} Z'_k \quad (3.8)$$

$$HAD_k = U_{Hk} \frac{\partial}{\partial x} (Z'_k - Z'_{k+1}) + \frac{g}{f_0} \left(\frac{\partial}{\partial x} Z'_k \right) \left(\frac{\partial}{\partial y} \bar{h}_k \right) = U_{Hk} \frac{\partial}{\partial x} (Z'_k - Z'_{k+1}) - \left(\frac{\partial}{\partial x} Z'_k \right) (U_k - U_{k+1}) \quad (3.9)$$

$$D_k = -\frac{\partial}{\partial x} \left[\frac{\partial}{\partial x} (u'_k v'_k) + \frac{\omega'_{k+1/2}(v'_{k+1} + v'_k) - \omega'_{k-1/2}(v'_k + v'_{k-1})}{2\Delta p} \right] \quad (3.10)$$

and

$$E_{k+1/2} = -\frac{\partial}{\partial x} \left[\frac{(u'_k + u'_{k+1})}{2} h'_{k+1/2} \right] + \frac{R}{c_p} \frac{1}{p_{k+1/2}} \omega'_{k+1/2} h'_{k+1/2} - \frac{1}{2 \cdot p_{k+1/2} \cdot \Delta p} [p_{k+1}(\omega'_{k+1/2} h'_{k+1/2} + \omega'_{k+1/2} h'_{k+1/2}) - p_k(\omega'_{k+1/2} h'_{k+1/2} + \omega'_{k-1/2} h'_{k-1/2})]. \quad (3.11)$$

The vertical derivative has already been replaced with finite difference.

In the numerical procedure for integrating the governing equations, it is implicitly assumed that the magnitude of a non-geostrophic component of wind is one order of magnitude less than that of a geostrophic one. (See Appendix C.)

DATA

In the present experiment, analytical patterns are dealt with instead of real data. In this connection, the height distribution, the vertical profile of the zonal mean velocity $U(p)$, and that of the zonal mean static stability $S(p)$ have to be specified.

Height field.—The following sinusoidal monochromatic wave pattern is given as the height field, i.e.,

$$Z(x, p, t) = Z_0(x, p, t) + Z_1(p) = Z'(p, t) \sin \left[\frac{2\pi}{L} x + \delta(p, t) \right] + Z_1(p) \quad (3.12)$$

We assume initially a uniform amplitude throughout the whole atmosphere regardless of p , i.e., $Z'(p, 0) = 100$ m. for the wave of wavelength 12,000 km., $Z'(p, 0) = 50$ m. for the wave of $L = 6,000$ km., and $Z'(p, 0) = 20$ m. for the wave of $L = 3,000$ km. These numerical values of the amplitude $Z'(p, 0)$ give almost the same amount of the eddy kinetic energy for three waves, respectively. (As an exception, a computation for the wave of $L = 6,000$ km. is made with $Z'(p, 0) = 100$ m.) Although this assumption seems to be too artificial, it is considered that the physical effect can be observed clearly by starting with the simple pattern rather than with the complicated one. Similarly, no vertical tilt of trough and ridge axes is assumed at initial time, i.e., $\delta(p, 0) = 0$ for all p . Since the absolute value of zonal mean height of each information level $Z_1(p)$ is not involved in the present computation, it is put to be zero. For some diagnostic studies, the realistic vertical distributions of the amplitude are prepared as is shown in figure 3.2. This is manufactured with reference to the several results of harmonic analysis by Eliassen [12], Teweles [31], and Muench [19]. Some values are assigned to $\delta(p, 0)$.

Vertical profile of $U(p)$.—For the initial value problem, a few artificial profiles of $U(p)$ are assumed. They are UI ,

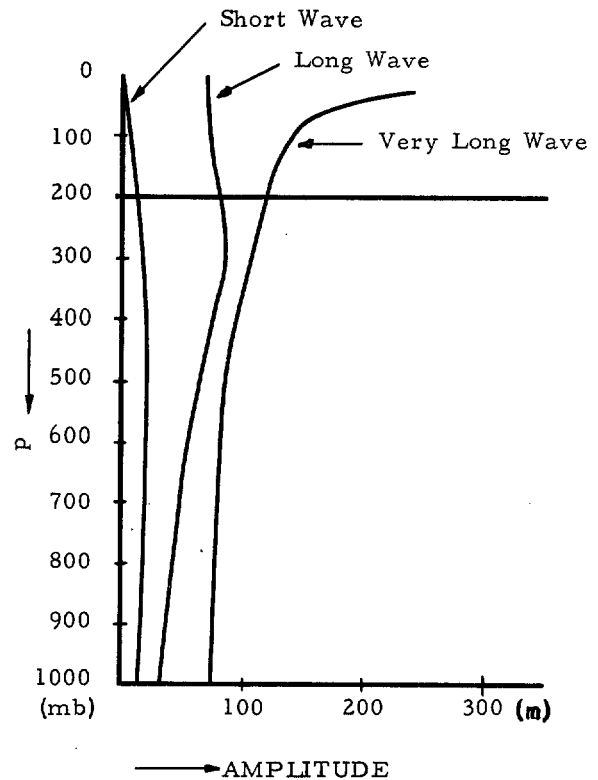


FIGURE 3.2.—The realistic vertical distribution of the amplitude of the three waves. From left to right, respectively, the amplitude for the short wave ($L = 3,000$ km.), that for the long wave ($L = 6,000$ km.), and that for the very long wave ($L = 12,000$ km.).

UII , and $UIII$ in figure 3.3 (a), (b), and (c), respectively. Some of them are also used in the diagnostic approach. The realistic profiles of $U(p)$ are adopted in the diagnostic study, which is obtained by Murakami [21], and illustrated in figure 3.3(d) as $U(35)$ and $U(60)$, which mean respectively the zonal mean wind at $35^\circ N.$ and $60^\circ N.$

Vertical profile of $S(p)$.—For all computations, the vertical distribution illustrated in figure 3.4 is used, which satisfies the following formula:

$$S(p) = \begin{cases} a \left(\frac{200}{p} \right)^2, & a = 0.443 \text{ for } 0 \leq p \leq 200 \text{ mb.}, \\ b \left(\frac{1000}{p} \right)^2, & b = 0.0272 \text{ for } 200 < p \leq 1000 \text{ mb.} \end{cases} \quad (3.13)$$

4. RESULTS OF NUMERICAL EXPERIMENTS

In this section, the results of the numerical solutions with the model depicted in a previous section will be shown. The problem is treated from two different approaches, that is, the diagnostic method and the prognostic method.

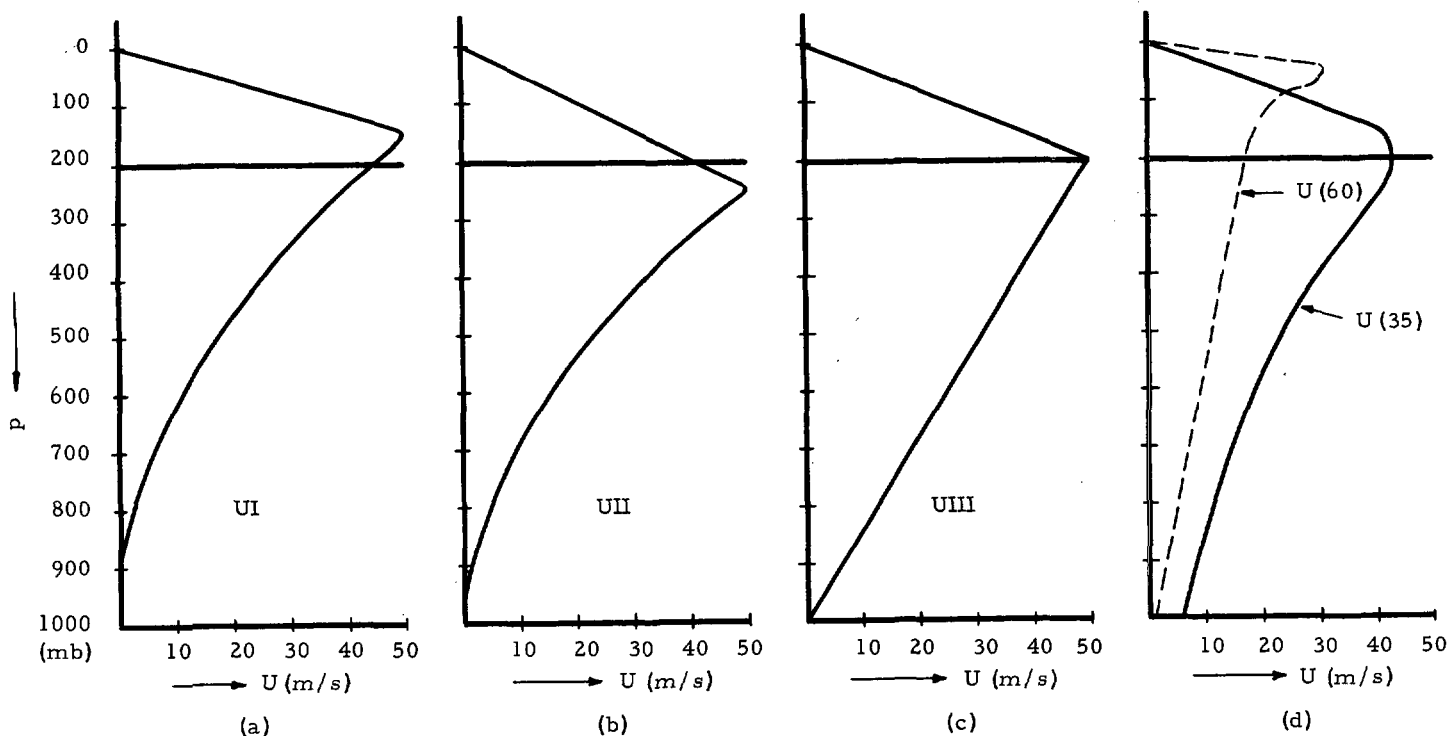


FIGURE 3.3.—The vertical profile of the zonal mean velocity U . (a) UI, (b) UII, (c) UIII, and (d) $U(35)$ and $U(60)$. The distributions (a) through (c) are artificial, and those in (d) are obtained by Murakami [21] from the observed data.

The former approach is adopted to obtain information on the vertical distributions of the interacting quantities for various combinations of basic parameters concerning the structure of the baroclinic disturbance. However, since physical parameters are assigned beforehand, the diagnostic study gives us only the interrelation between the interacting quantities and the basic parameters. To proceed in a more general study, a numerical prediction with the computational model is performed. Because of the restriction of linearization, the forecast is terminated after a fixed period, say, 24 hr. Although the forecast is started with specific initial data, i.e., no tilt of the wave axes and uniform amplitude, the prognostic patterns after 24 hr. show good resemblance to the typical structure of the waves in the middle-latitude westerlies. In this connection, the predicted vertical distributions of the interacting quantities may be considered to have physical significance to depict the dynamical coupling between the lower stratosphere and the troposphere.

RESULTS OF THE DIAGNOSTIC RESEARCH

In the diagnostic study with the computational model, equation (3.5) is solved iteratively for ω' from a prescribed pattern of Z' (or ϕ') and a set of physical parameters S , U , etc. (See Appendix C.) The height field is determined by equation (3.12) with the vertical profiles of amplitudes shown in figure 3.2 respectively for the three representative waves. As the vertical distributions of the zonal mean wind, $U(35)$ and $U(60)$ in figure 3.3 (d) are adopted.

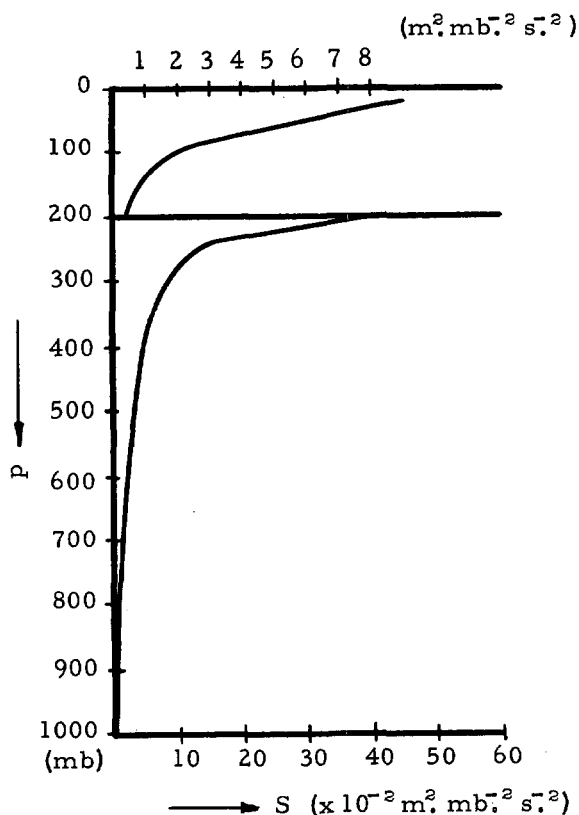


FIGURE 3.4.—The vertical profile of the artificial zonal mean static stability, S . Numbers on the lower abscissa are for S at 1000 mb. $\geq p \geq 200$ mb. and those on the upper one are for S at 200 mb. $> p > 0$ mb.

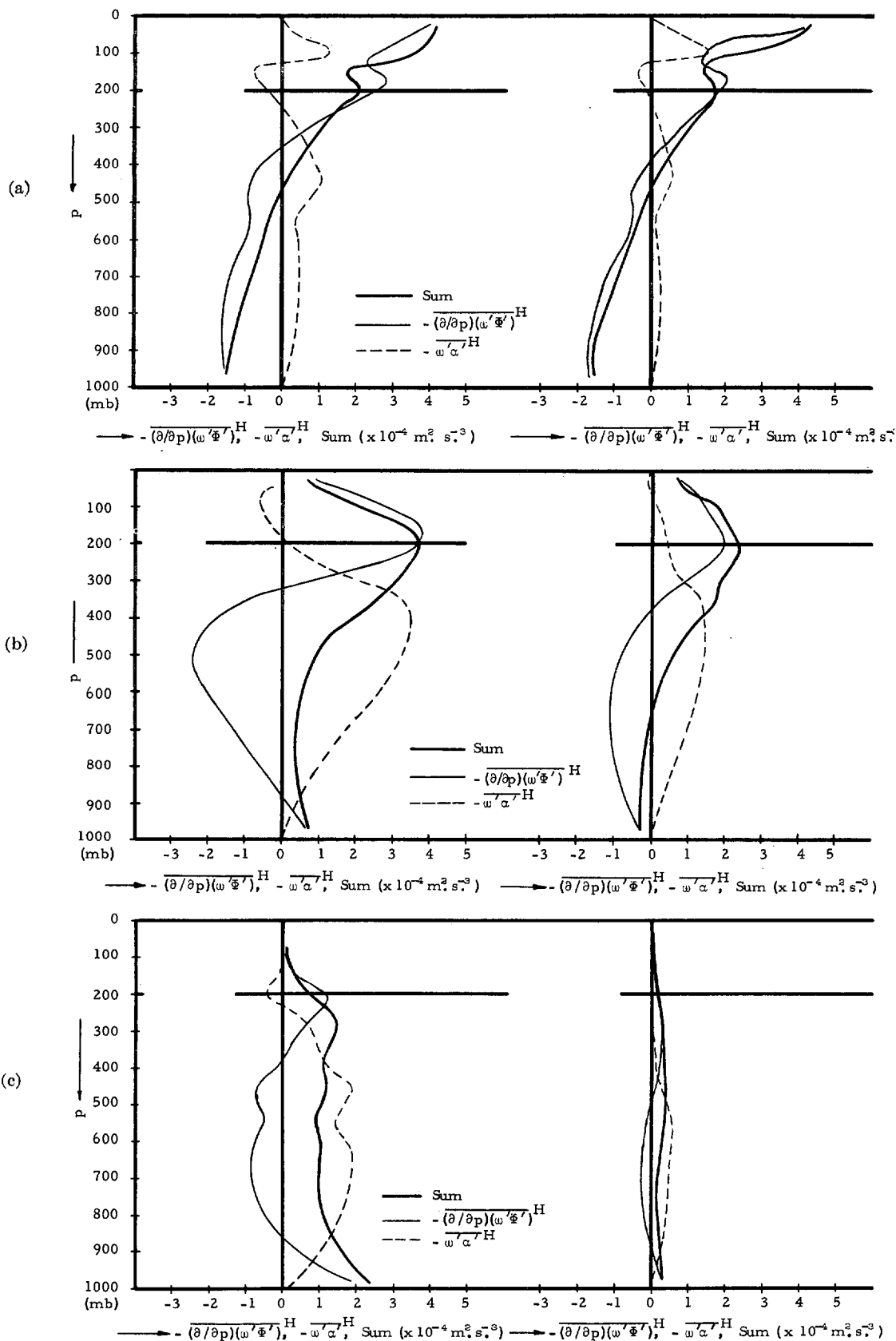


FIGURE 4.1.—The diagnostic numerical solution with the linearized 20-level model, of the redistribution term $-\overline{\partial(\omega'\phi')/\partial p}^H$ (thin solid line), that of the conversion term $-\overline{w'\alpha'}^H$ (thin dashed line), and that of the sum of both terms or the generation term (heavy solid line). The left figure shows the results for $U(35)$ and the right one for $U(60)$. (a) The diagram for $L=12,000$ km., (b) that for $L=6,000$ km., and (c) that for $L=3,000$ km.

Figures 4.1 (a) through (c) show the vertical distribution of $-\frac{\partial(\omega'\phi')}{\partial p}^H - \omega'\alpha'^H$, and the sum of both terms for the three characteristic disturbances respectively. The vertical tilt is assigned as $\delta = -L/4$ which means the westward inclination with increase in the height to the extent of a quarter of a wavelength for the whole depth of the atmosphere.

For the profiles of U at 35°N . and 60°N ., the eddy kinetic energy is generated mostly in a similar manner, but the amount is different. This is commonly seen for all the three waves taken up here. The very long wave mostly contributes to the energy generation in the stratosphere, and the synoptic-scale long wave has the maximum generation around the 200-mb. surface which is regarded as the level of the tropopause in the experiment. The redistribution term has a similar magnitude at the tropopause for the two larger-scale waves. The predominance of the contribution by the ultra-long wave in the stratosphere is mainly due to the large value of the amplitude of the wave there. The diagnostic results for amplitude which is uniform in the vertical shows that the contribution by the very long wave to the generation term is much smaller than the case illustrated in figure 4.1(a). The prognostic results which will be described later also do not show the large amount of the amplitude of the very long wave in the stratosphere. The determination of a realistic profile of the amplitude is a problem beyond the present work, and further progress of our understanding on the dynamics of the ultra-long wave is urgently needed.

Contrary to the case of these larger-scale disturbances, the wave of wavelength 3,000 km. relates little to the budget of the eddy kinetic energy in the lower stratosphere. In the middle troposphere, the conversion term contributes to increase eddy kinetic energy. On the other hand, the redistribution term decreases the eddy kinetic energy to minimize the generation term for the very long wave and the long wave. For the short wave, there is almost no generation in the lower stratosphere, but the relatively large rate of the increase in eddy kinetic energy is observed in the middle troposphere. Accordingly, the spectrum distribution of the waves in the atmosphere would be important. The frictional forces ignored in the diagnostic experiment may also change the situation.

Although it is not illustrated here, an estimate of the vertical transport of eddy kinetic energy $-\frac{\partial(\omega K')}{\partial p}^H$ shows one or more order of magnitude smaller than the other interacting quantities considered here, as has been pointed out by many authors. Furthermore, the following results are obtained from the diagnostic numerical study and are supported by the simple analytical solutions (See Appendix A.)

(1) The tilt of the disturbances is crucial in determining the sign of the interacting quantities. In the case of no inclination, no generation results. The results so far illustrated are characteristic of the waves which tilt westward with altitude. The disturbances tilting leeward with increase in height change the sign of the interacting quantities.

(2) The absolute magnitudes of the interacting quantities are approximately in proportion to the degree of inclination of the wave axes and the absolute size of the amplitude of waves.

(3) The very long wave is remarkably influenced by the β -effect. The β -term promotes the contribution of the redistribution term to increase eddy kinetic energy in the upper half of the atmosphere and suppresses that in the lower half of the troposphere, and even makes the sign of the generation term negative. The effect of the β -term weakens for shorter waves.

(4) The vertical flux of geopotential $-\overline{\omega'\phi'}^H$ is positive and has a similar magnitude for the very long wave and the long wave throughout the lower stratosphere and the upper troposphere.

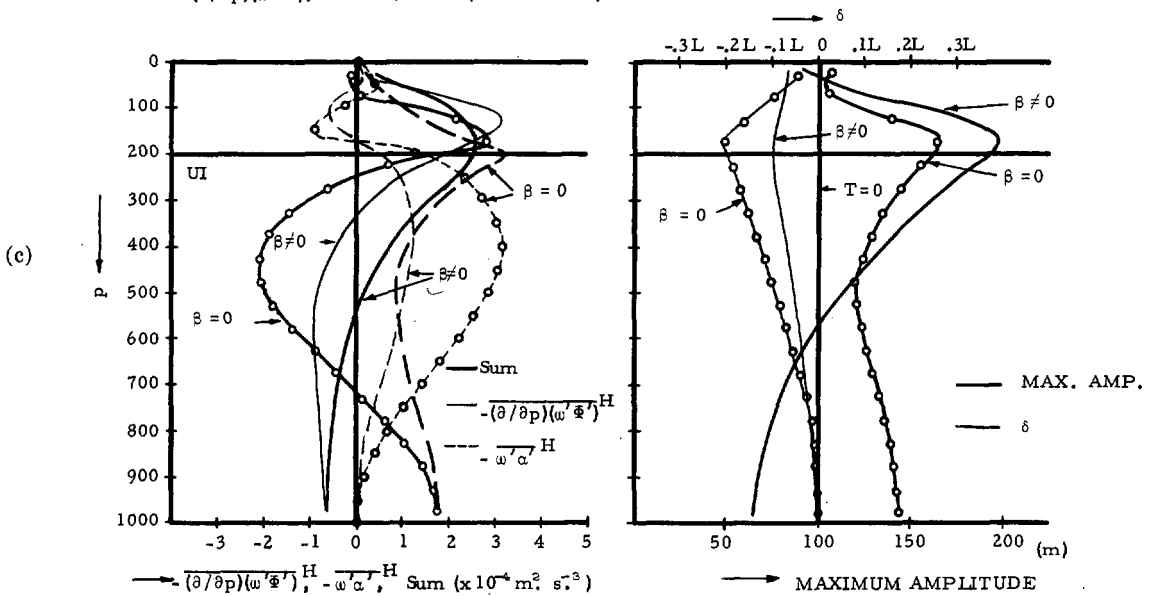
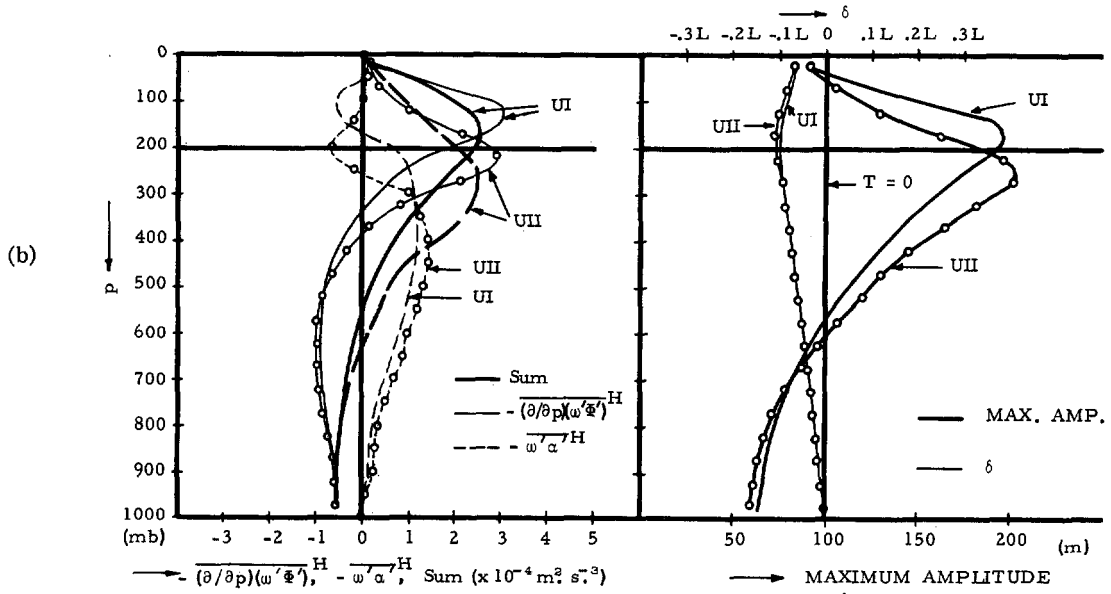
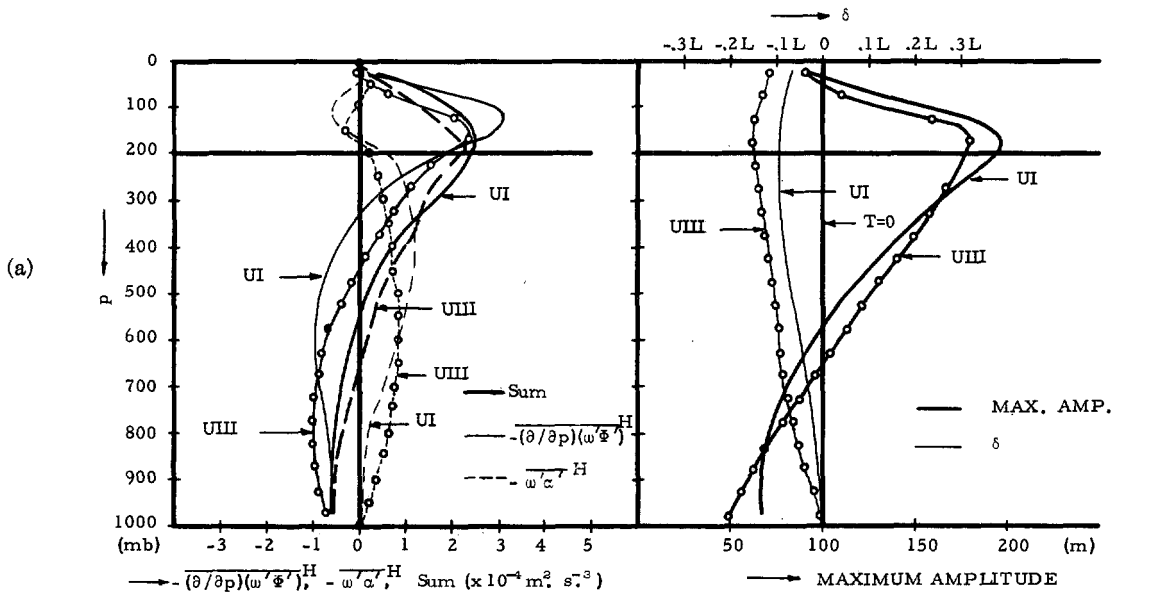
Although the results obtained in the diagnostic approach give us the physical image of the interaction, it should be noted that the vertical profiles of the amplitude and those of the degree of inclination of wave axes are assumed beforehand. Furthermore, the solution demonstrates no more than an instantaneous state under the prescribed pattern. To proceed further, the problem has to be treated from the prognostic viewpoint.

RESULTS OF THE PROGNOSTIC RESEARCH

The same pattern as is adopted for the diagnostic approach is used, but a wave axis is set straight upward at the initial time. A grid interval of 200 km. is used. The prognostic profiles of the interacting quantities after 24 hr. for the wave of wavelength 12,000 km. are illustrated in figure 4.2. The interacting quantities are shown on the left and the vertical profiles of maximum amplitudes of the waves and those of the phase on the right.

Figure 4.2 (a) indicates a comparison between the results of the cases where $U=UI$ and $U=UIII$. (See fig. 3.3.) The difference between these two zonal mean currents is the curvature of the vertical wind shear, i.e., for UI , $\partial^2 U/\partial p^2 > 0$, and for $UIII$, $\partial^2 U/\partial p^2 = 0$. First of all the two prognostic distributions agree with the diagnostic results. The effect of $\partial^2 U/\partial p^2$ is such that it increases the magnitude of the redistribution term in the lower stratosphere and promotes the energy conversion from the eddy available potential energy to the eddy kinetic energy in the upper half of the troposphere. In view of the eddy kinetic energy generation, however, this difference is not remarkable. The redistribution term has its maximum value above the level of the maximum generation. Between these two maximum levels, the level of the strongest zonal flow and the level of the largest growth rate are observed. (Compare the left-hand side and the right-hand side of figure 4.2 (a).)

Next, the effect on the vertical profiles of the interacting quantities, of the height where U has its maximum value is examined (fig. 4.2(b)). As is observed in figure 3.3, the level of maximum zonal mean wind in UII is higher than that in UI . The two levels differ in height an amount ΔH which is equivalent to 100 mb. in pressure. As a result, the level of the maximum in the redistribution term and that



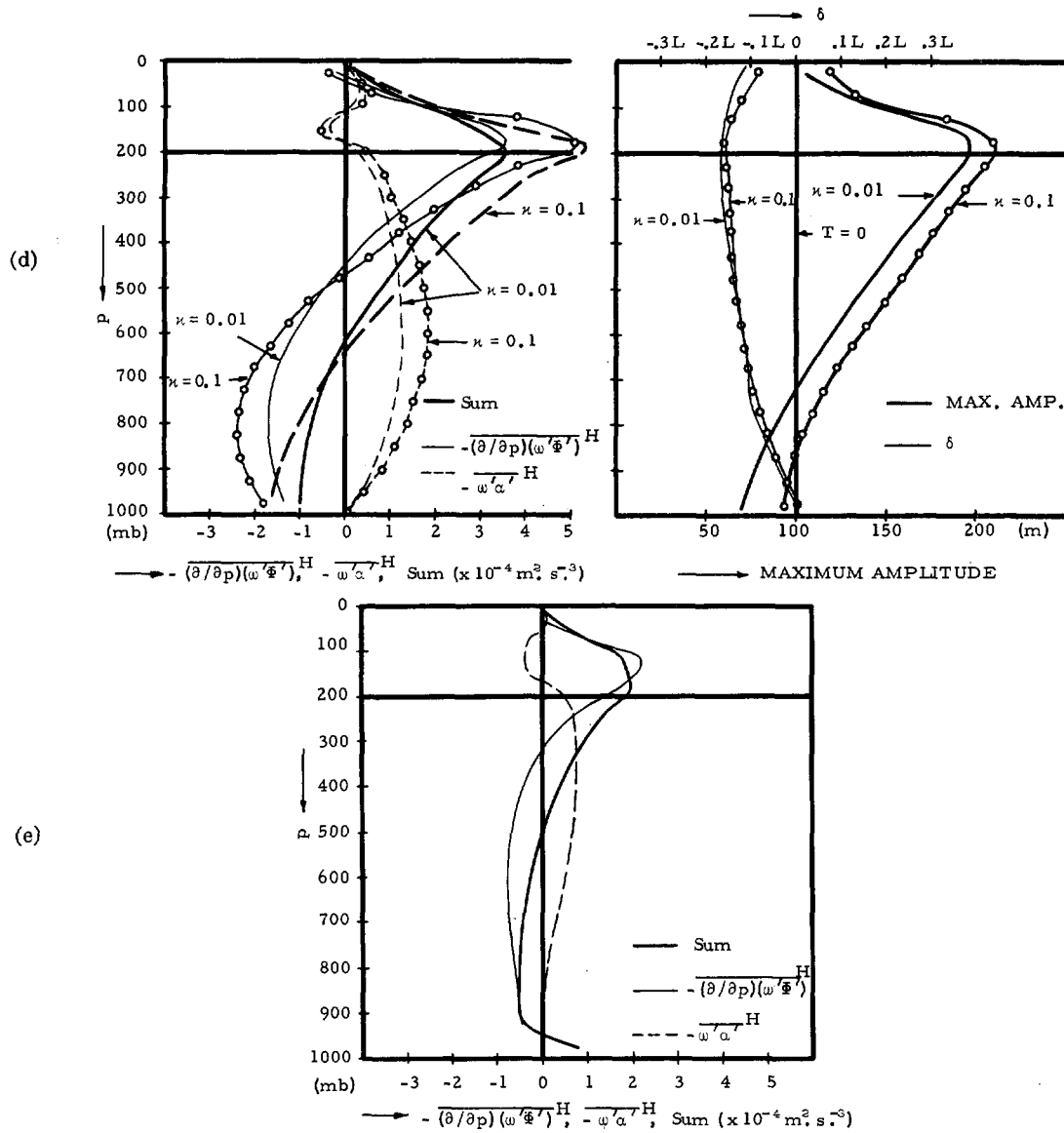


FIGURE 4.2.—Predicted profiles of the interacting quantities, $-\frac{\partial(\omega'\phi')}{\partial p}H$, $-\omega'\alpha'$, and the sum of both terms (on the left), and the computed vertical distribution of the maximum amplitude and the phase (on the right). The results for the very long wave of wavelength 12,000 km. with $Z'=100$ m. and $\gamma=0$ at the initial time. (a) The results for UI and UIII. (b) The results for UI and UII. (c) The results for $\beta=0$ and $\beta\neq 0$ with UI. (d) The results for $\kappa=0.1$ and $\kappa=0.01$ with UIII. (e) The results for UI with vertical sub-grid-scale diffusion. On the left-hand side, the thin solid line shows the term $-\frac{\partial(\omega'\phi')}{\partial p}H$ (the results for the latter cases in (a) through (d) connect circles). The thin dashed line indicates $-\omega'\alpha'$. The thick solid curve illustrates the generation term (the results for the latter cases in (a) through (d) are shown with the thick broken line). On the right-hand side, the thick solid line shows the maximum amplitude, the thin solid line the phase.

in the generation term in the case of $U=UII$ are approximately ΔH higher than that in the case of $U=UI$. Concerning the absolute magnitude of these quantities, the results in the two cases are similar for the very long wave. About the effect of the meridional variation of the Coriolis parameter, the β -term, in general, leads to a similar influence on the vertical profiles of the quantities in both the prediction and diagnostic studies. (See fig. 4.2(c).) There is, however, an important discrepancy. In the forecast, the case of $\beta=0$ results in, at the tropopause, the same amount of the redistribution and a greater magnitude of the conversion than in the case $\beta \neq 0$, to lead to the sharp maximum in the generation. On the contrary, the diagnostic approach does not display this trend. The very long wave shows a fictitious westward retrogression in the atmosphere when there is no vertically integrated divergence (Wolf [34], Cressman [9], Wiin-Nielsen [33]). The numerical model adopted here is the one which may give rise to this error for horizontal movement of ultra-long waves. To avoid the error in a simple manner, we introduce artificial total divergence which is assumed to be proportional to the height tendency with time at the lowest level of the atmosphere. Figure 4.2(d) shows the results for the two different magnitudes of the total divergence, where κ indicates the coefficient of the proportion in the form

$$\frac{1}{P} \int_0^{1000} \nabla \cdot \mathbf{V} dp \propto -\kappa \left(\frac{\partial}{\partial t} Z \right)_{p=975}, \quad P=1000 \text{ mb.}$$

The vertical profile $UIII$ is used for the zonal mean wind. Except for the absolute magnitude of the interacting variables, the case of $\kappa=0.1$ and that of $\kappa=0.01$ result in similar patterns. In comparison with the case $\kappa=0$, the two cases of $\kappa \neq 0$ have sharper curvature around the maximum of the redistribution term and that of the generation term. This suggests to us that the blocking effect for the fictitious westward movement leads to an intensification of the eddy kinetic energy in the lower stratosphere, which is redistributed by the term $-\overline{\partial(\omega'\phi')/\partial p}^H$. Although there is not enough information on the vertical distribution of amplitude of the very long wave in the stratosphere, it should be remarked that the predicted vertical profiles of amplitude seem to be different from those of observation, i.e., the computed amplitude has the vertical maximum around the level of the strongest zonal mean flow, but in the real atmosphere the increase in amplitude of the very long wave is usually observed with increase in altitude in the lower stratosphere. The reason for this discrepancy may be related to the mechanism of maintenance of the very long wave. To examine the effect of the dissipational force, a computation with the vertical diffusion due to the Austausch coefficient is performed. Figure 4.2(e) shows the results with dissipation. The effect makes the redistribution term predominant in the lower layer. This trend was already pointed out by Arakawa [1], [2] in relation to the angular momentum

balance in the middle-latitude westerlies. As is easily expected, the effect of the friction is more conspicuous for the shorter waves.

Now, let us turn to look at the case of the long wave of wavelength 6,000 km. Figure 4.3(a) demonstrates the result for $U=UI$. The levels of the maximum redistribution term and of the maximum generation term shift downward in comparison with the result for the very long wave. Agreement of the predicted profiles with those obtained by the diagnostic approach is very good. The results in the case of $U=UI$ and those of $U=UII$ are shown in figure 4.3(b). (As an initial uniform amplitude, 100 m. is used to exaggerate the difference. The double initial amplitude leads to a double value of the interacting quantities.) The difference in the results due to the difference in U appears similar to that in the case of the very long wave, but the magnitude of the discrepancy increases for the shorter waves. The profile in the case of $U=UII$ results in a sharper curve around the maximum generation near the tropopause and increases the magnitude of the maximum. This means that the high sensitivity of the unstable baroclinic wave to the vertical wind shear is reflected in the interacting quantities. (See the vertical profile of the maximum amplitude in the right-hand side of fig. 4.3(b).)

The effect of the dissipation due to the vertical gross viscosity is notable for this wave as is illustrated in figure 4.3(c). The rate of the redistribution is sharply increased in the lowest level. Inclusion of the lateral diffusion term in the governing equations does not make any significant change in the results, though the profiles are not shown here.

The profiles for the short wave are shown in figure 4.4. The wave of the wavelength which is 3,000 km. also indicates high sensitivity to the vertical wind shear. Again, the prognostic results agree well with those by the diagnostic approach. It should be noted that the predicted vertical distribution of the interacting quantities is essentially different from the profiles in the two cases of the longer waves. For the vertical profile of zonal mean current which has the level of the strongest wind above the tropopause, the redistribution term shows negative near the tropopause, but the generation is still positive. This suggests to us the different types of the dynamical interaction. The downward redistribution in the mid-troposphere is also more remarkable in this case than the other two cases. The results for the vertical gross viscosity are shown in figure 4.4(b). The same trend as that for the long wave is observed. Concerning the absolute amount of the generation in the lowest layer, the long wave and the short wave give rise to a similar magnitude which is larger than that due to the very long wave.

Finally, figure 4.5 indicates the predicted profiles of $-\overline{\omega'\phi'}^H$ for the three waves. One of the most marked differences from the diagnostic case is that the long wave leads to a strong vertical flux of geopotential through the tropopause. As far as the forecast made here is concerned,

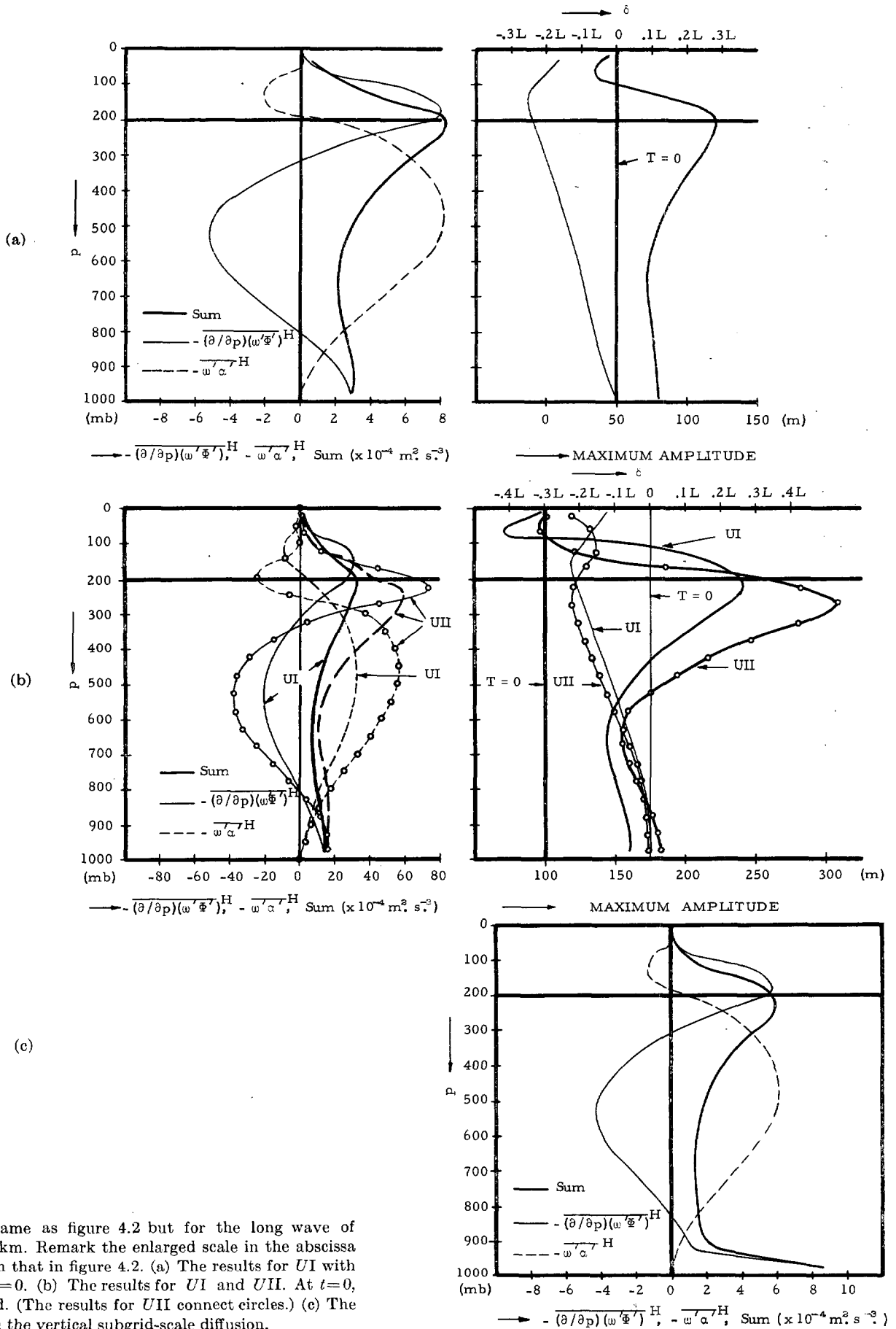


FIGURE 4.3.—The same as figure 4.2 but for the long wave of wavelength 6,000 km. Remark the enlarged scale in the abscissa in comparison with that in figure 4.2. (a) The results for UI with $Z'=50$ m., and $\gamma=0$. (b) The results for UI and UII. At $t=0$, $Z'=100$ m. is used. (The results for UII connect circles.) (c) The results for UI with the vertical subgrid-scale diffusion.

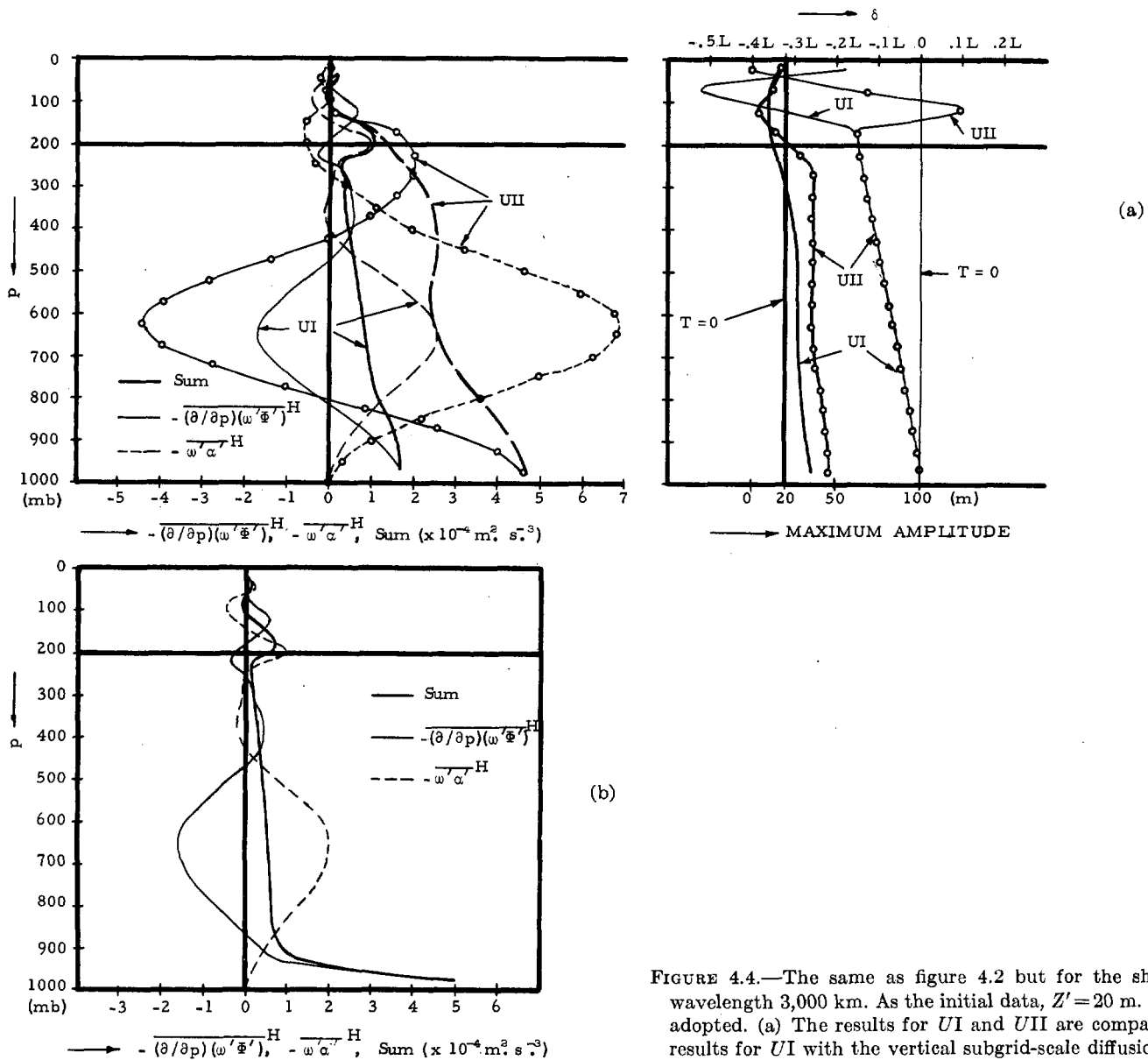


FIGURE 4.4.—The same as figure 4.2 but for the short wave of wavelength 3,000 km. As the initial data, $Z' = 20$ m. and $\gamma = 0$ are adopted. (a) The results for UI and UII are compared. (b) The results for UI with the vertical subgrid-scale diffusion.

the synoptic scale disturbance is the most efficient in generating the eddy kinetic energy in the lower stratosphere. In the lower half of the troposphere, the downward flux is also more conspicuous than that in the diagnostic study. The effect of vertical diffusion on the vertical flux of geopotential appears to promote intensity of the downward flux. (See fig. 4.5(b).) On the contrary, the upward flux into the stratosphere is decreased. These trends are more or less common to the three characteristic waves.

5. DISCUSSION OF THE RESULTS

As a supplement to the numerical experiment, a simple analytical solution is obtained for a quasi-geostrophic system. (See Appendix A.) The analytical expressions of the interacting quantities agree reasonably well with the numerical results and indicate the interrelation with

various combinations of physical parameters may be interpreted as for the numerical results.

Next, to compare the present results with those obtained by the more elaborate computational model, the vertical profiles obtained by Smagorinsky, Manabe, and Holloway [29] are referred to in figure 5.1. The patterns show the 70-day average state. Since their computational model contains neither mountains nor sensible heat supply from the ocean, the results could be interpreted to indicate the statistical mean state of the dynamical interplay due to transient disturbances. From the viewpoint of the coupling between the lower stratosphere and the troposphere, the sharp predominant generation of eddy kinetic energy is observed around 200 mb. When the numerical solution by the general circulation model is compared with that by the present experiment, it follows that both solutions

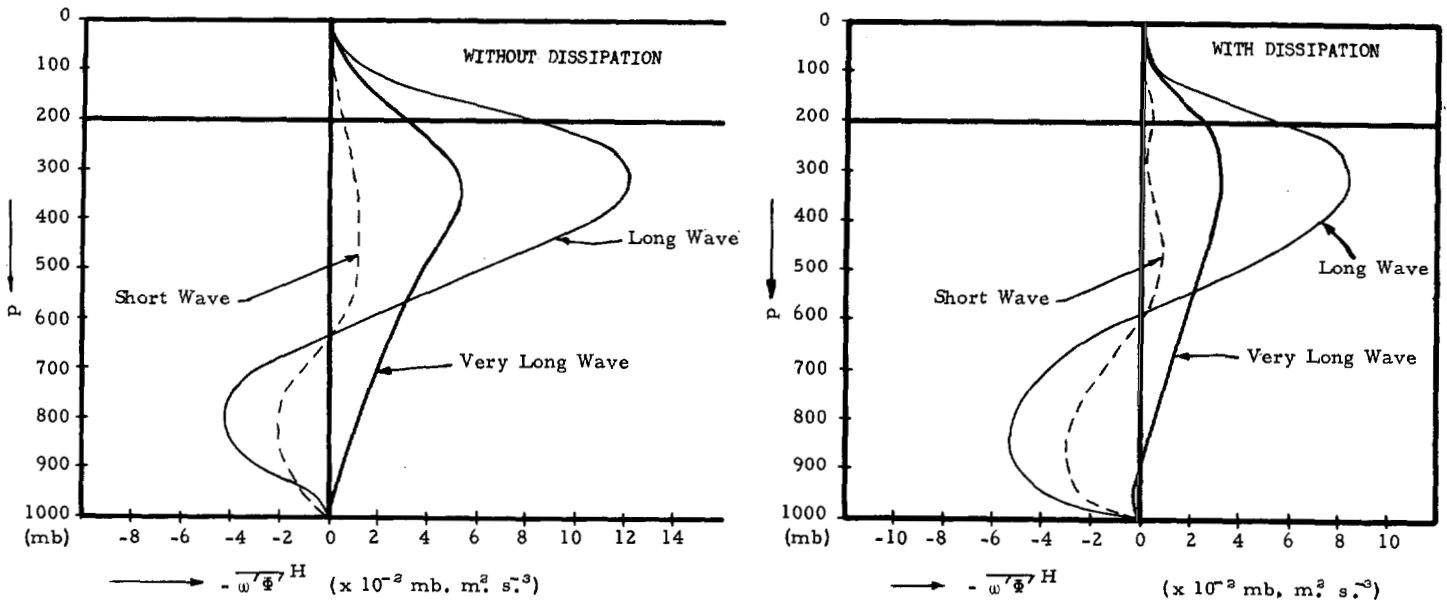


FIGURE 4.5.—(a) The vertical profiles of the predicted values of $-\overline{\omega' \Phi'}^H$ for the cases in figure 4.2 (a) and (b) for UI (the very long wave); in figure 4.3(a) for UI (the long wave), and in figure 4.4(a) for UI (the short wave). Without dissipation. (b) The vertical distribution of the computed flux, $-\overline{\omega' \Phi'}^H$, for the cases in figure 4.2(e), figure 4.3(c), and figure 4.4(b). With dissipation.

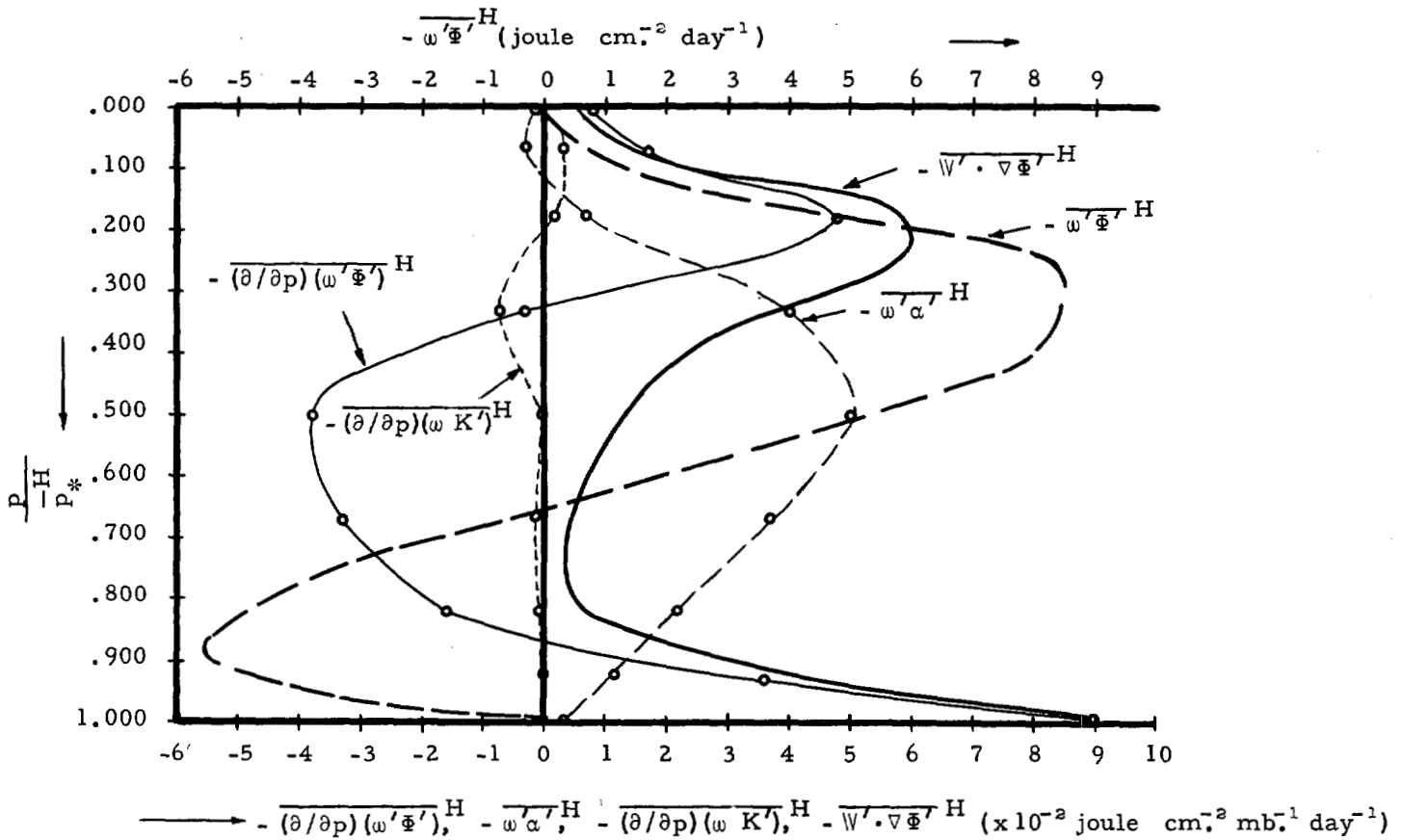


FIGURE 5.1.—The vertical distribution of the horizontal mean value of the rate of generation $-\overline{V' \cdot \nabla \Phi'}^H$, and its components by the numerical model for the study of the general circulation of the atmosphere. (Smagorinsky, Manabe, and Holloway [29].)

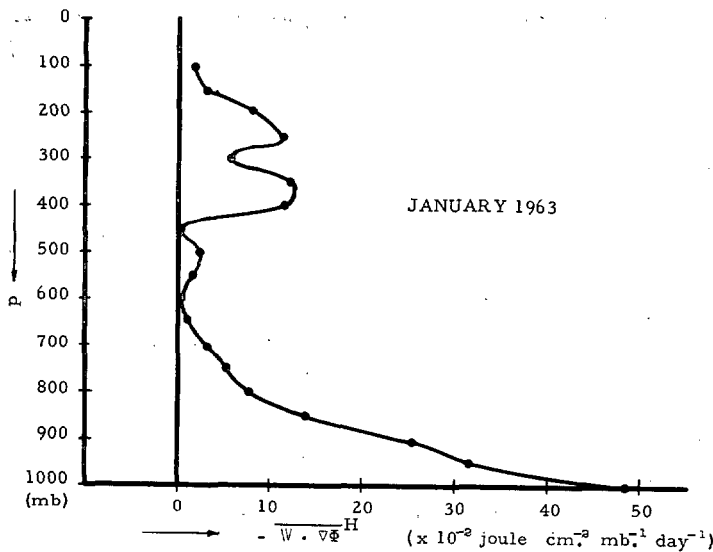


FIGURE 5.2.—The vertical profile of the area averaged value of the rate of the generation $-\mathbf{V} \cdot \nabla \phi^H$ obtained from the observation for January 1963. (Kung [15]).

look alike and especially the results of the long wave of wavelength 6,000 km. shows the best resemblance to the results by the more elaborate model. It should be pointed out that the mechanism which presumably transforms the eddy kinetic energy generated through the medium-scale wave to that of the ultra-long wave in the lower stratosphere is not revealed.

Numerical analysis of the energy generation in the real atmosphere with observation of wind and geopotential fields is done by Kung [15]. Monthly mean vertical profiles of the coupling variables for January 1963 are illustrated in figure 5.2. It should be understood that his results include contributions from both the transient and stationary waves. To a close approximation the profiles he obtained from the real atmosphere agree with those from the numerical simulation. One cannot estimate at once separately the contributions from the transient wave and from the stationary wave, but at least it may be emphasized that a considerable amount of the generation throughout the lower stratosphere and the upper troposphere is carried out by moving disturbances. The time sequential diagrams of the generation in the real atmospheric layers, which are also obtained by Kung [15], show frequent variations of the absolute value and changes of the sign in the daily computed values. These short-period oscillations seem to be related to activities and behaviors of migratory troughs and ridges.

The reasonable agreement of the present results with the other two studies suggests to us that the essential factors which determine the general aspect of the dynamical coupling are included in the present simple experiment. The factors are the inclination of wave axes (hence, the meridional transport of sensible heat), the

vertical wind shear, the vertical profile of static stability, the total non-vanishing divergence, the β -effect, and the dissipation.

The maximum values of the generation term in the upper atmosphere are compared in table 5.1. As an example from the present study, the diagnostic study is used, which treats the long wave ($L=6,000$ km.) for the realistic profile of the amplitude and $U=U(35)$. The results from the different authors are of the same order of magnitude. The amount of the vertical flux of geopotential through the boundary surface and between the lower stratosphere and the troposphere are compared in table 5.2. As the observation in the real atmosphere, the monthly mean of January 1958, prepared by Miyakoda [18], is adopted. The pressure interaction term computed from the three-month mean values of January–March, 1958, as obtained by Oort [25], is also cited. Miyakoda [18] processed the height field to obtain all motion fields needed for the numerical analysis of the sudden warming phenomenon. Since Oort [25] dealt with the three-month mean value, his result appears very small. The other three estimates are of similar size. It should be remembered that an absolute amount of the net flux into the stratosphere depends very much on the level chosen as the boundary surface between the lower stratosphere and the troposphere.

Concerning the contribution by the stationary waves, Eliassen and Palm [11] show for a quasi-geostrophic wave that

$$-\overline{\omega' \phi'}^H = U \left(\frac{fR}{\sigma p} \right) \overline{T' v'}^H, \quad (5.1)$$

and mention that “long quasi-geostrophic stationary waves will transport wave energy upward if the flux of sensible heat is directed northwards, i.e., if the waves tilt westward with height (assuming $U > 0$, $\sigma > 0$).” The term on the right-hand side of equation (5.1), however, does not appear in the case of migratory disturbances, because this term is attributed to the heat advection term by the zonal basic current in the thermal equation, which is cancelled out by the corresponding term in the vorticity equation when we solve the ω -equation to obtain $-\overline{\omega' \phi'}^H$. (See Appendix A.) In this respect, although both the transient and stationary waves have the vertical flux of geopotential, the physical relation between the wave tilt and the energy transfer is quite different in the two waves.

Finally, some comments will be made on the computational model. The multi-level balanced baroclinic model adopted in the present experiment is capable of a comprehensive treatment of the waves in a broad range of the wave spectrum. Comparison of the present results with those of the same computation with the quasi-geostrophic model indicates little difference between the very long wave and long wave regimes. On the other hand, for the wave of shortest wavelength, a definite difference is noticed between the two models.

TABLE 5.1.—Comparison of the maximum value of the energy generation term in the upper atmosphere

Authors	Energy generation (Unit: 10^{-2} joule cm^{-2} mb^{-1} day^{-1})	Level of the maximum value (mb.)	Area	Notes
Smagorinsky, Manabe, and Holloway [29].....	5	200	Northern Hemisphere.....	70-day mean of the daily values of the numerical simulation; annual mean.
Kung [15].....	12 13	250 350	North America.....	January 1963; monthly mean of the daily values.
The present computation.....	3.5	200	One-dimensional space, 12,000 km. in size.	The case of the diagnostic numerical approach for the long wave of wavelength 6,000 km. The realistic distribution of the amplitude and the zonal mean flow are used. Roughly winter state.

TABLE 5.2.—Comparison of the amount of the vertical flux of geopotential at the boundary surface between the lower stratosphere and the troposphere

Authors	Pressure of the boundary level (mb.)	$-\overline{\omega'\phi'}H$ (Unit: joule cm^{-2} day^{-1})	Area	Notes
Smagorinsky, Manabe, and Holloway [29].....	200	6	Northern Hemisphere.....	70-day mean of the daily values of the numerical simulation; annual mean.
Miyakoda [18].....	189	2.6	Northern Hemisphere, 90° N.~30° N.	January 1958; monthly mean of the daily values.
The present computation.....	200	4.5	One-dimensional space, 12,000 km. in size.	The case of the diagnostic numerical approach for the long wave of wavelength 6,000 km. The realistic distribution of the amplitude and the zonal mean flow are used. Roughly winter state.
Oort [25].....	75	0.04	Northern Hemisphere.....	Computed from the 3-month mean chart, Jan.-Mar. 1958.

6. SUMMARY

The energetic process which links the lower stratosphere and the troposphere is pursued by solving numerically a 20-level linearized baroclinic equation. The cases treated here correspond to those at the middle latitudes and roughly in winter. The space-mean conversion from eddy available potential energy to eddy kinetic energy occurs mostly in the middle troposphere. Simultaneously the area-average redistribution term acts to reduce the eddy kinetic energy in the mid-troposphere and to increase it around the tropopause or in the lower stratosphere. Thus, the time change of eddy kinetic energy becomes a maximum near the tropopause or above it. (The increase in the eddy kinetic energy in the lower stratosphere, which is connected with the tropospheric motions in this manner, feeds the energetics there.)

The above-mentioned process is investigated with relation to the structure of the baroclinic disturbances. The vertical profiles of the interacting quantities, i.e., $-\overline{\partial(\omega'\phi')/\partial p^H}$, $-\overline{\omega'\alpha'^H}$, the sum of both terms, and $-\overline{\omega'\phi'^H}$, are obtained by numerical time integration with the 20-level balanced baroclinic model. The vertical transport term $-\overline{\partial(\omega K')/\partial p^H}$ is ignored because it is very small. The diagnostic studies with the computational model and with the simple analytical method are performed as a supplement to the prognostic research.

The main results are summarized as follows:

(1) The vertical tilt of a wave axis determines the sign of the interacting quantities, i.e., $-\overline{\partial(\omega'\phi')/\partial p^H}$, $-\overline{\omega'\alpha'^H}$, $-\overline{\mathbf{V}'\cdot\nabla\phi'^H}$, and $-\overline{\omega'\phi'^H}$. The windward inclination of axes with increase in altitude promotes the increase in the eddy kinetic energy in the lower stratosphere and the upper troposphere, in the case $\partial U/\partial p < 0$. A leeward tilt results in the reverse sense. The vertical straight axis leads to no change in the eddy kinetic energy. The degree of the vertical inclination is proportional to the absolute amount of the interacting quantities.

(2) The amplitude of the wave, the wavelength, $\partial U/\partial p$, and the Coriolis parameter are directly involved in determining the magnitude of the interacting quantities.

(3) In the range of the realistic distribution, the effect of the zonal mean static stability on the interacting quantities is not predominant.

(4) For the ultra-long wave, the effect of the total non-vanishing divergence appears to promote the energetic interaction in the atmospheric layers.

(5) The β -effect increases the magnitude of the redistribution term in the upper troposphere and decreases it in the lower troposphere for the windward inclined wave.

(6) The role played by the dissipation is such that the vertical gross viscosity in the lower layer leads to the

downward redistribution of eddy kinetic energy, especially, in the lowest layer.

(7) The present conclusions agree well with results obtained by the numerical simulation of the general circulation of the atmosphere and by numerical analysis of observed data. In the earth's atmosphere, the general circulation requires the predominance of the westward tilt of wave axes with height in the middle latitudes, so that the eddy kinetic energy is converted from the eddy available potential energy in the middle troposphere and redistributed so as to be maximum near or above the tropopause.

APPENDIX A

A SIMPLE ANALYTICAL EXPRESSION OF THE INTERACTING QUANTITIES

An analytical solution for the ω -equation is obtained. As mentioned in the Introduction, the quasi-geostrophic approximation is used for this purpose. The quasi-geostrophic ω -equation reads

$$\nabla^2 \omega + \frac{f_0^2}{S} \frac{\partial^2 \omega}{\partial p^2} = \frac{1}{S} \left[f_0 \frac{\partial}{\partial p} \left(u_g \frac{\partial \eta_g}{\partial x} + v_g \frac{\partial \eta_g}{\partial y} \right) - \nabla^2 \left(u_g \frac{\partial \phi_p}{\partial x} + v_g \frac{\partial \phi_p}{\partial y} \right) \right], \quad (\text{A.1})$$

where $\eta_g = \frac{1}{f_0} \nabla^2 \phi + f$, $u_g = -\frac{1}{f_0} \frac{\partial \phi}{\partial y}$, $v_g = \frac{1}{f_0} \frac{\partial \phi}{\partial x}$, and $\phi_p = \frac{\partial \phi}{\partial p}$.

We assume that motions are confined in x, p -plane and variables are separated into the zonal mean value and the deviation from it. (The horizontal mean $\overline{(\)}^H$ coincides with the zonal average $\overline{(\)}^X$ in the present case, and hereafter will be denoted as $\overline{(\)}$.) Namely, we put

$$\begin{aligned} \omega &= \omega'(x, p, t), \quad \phi = \phi'(x, p, t) + \bar{\phi}(y, p), \quad \frac{\partial^2 \bar{\phi}}{\partial y^2} = 0, \\ \frac{\partial^2 \bar{\phi}}{\partial p \partial y^2} &= 0, \quad u_g = U(p), \quad v_g = \frac{1}{f_0} \frac{\partial \phi'}{\partial x}, \quad \phi_p = \phi'_p(x, p, t) + \bar{\phi}_p(y, p), \\ -f_0 \frac{\partial U}{\partial p} &= \frac{\partial}{\partial y} \bar{\phi}_p, \quad S = S(p), \quad \text{and } f(y) = f_0 + \beta y. \end{aligned}$$

Equation (A.1) is simplified to

$$\frac{S}{f_0^2} \frac{\partial^2}{\partial x^2} \omega' + \frac{\partial^2 \omega'}{\partial p^2} = \frac{1}{f_0} \left\{ 2 \frac{\partial U}{\partial p} \frac{\partial^2}{\partial x^2} v'_g + \beta \frac{\partial v'_g}{\partial p} \right\}. \quad (\text{A.2})$$

It should be noted that a contribution from the Laplacian of a zonal advection of the perturbed heat is cancelled out with a part of the vertical shear of the velocity advection. This situation makes an essential difference between the present treatment of the problem and the study of the vertical flux of geopotential due to the stationary waves.

For the sake of simplicity, we further assume that $S(p) = \text{constant} = S_0$, $a = 2f_0 \frac{\partial U}{\partial p} = \text{constant} (<0)$, $b = f_0 \beta$, $\phi = \phi_0 \sin(kx + lp)$, $k = 2\pi/L$, $l = \pi\gamma/P$, $P = 1000$ mb. ($\gamma < 0$ for westward (windward) tilt with altitude and $\gamma > 0$ for eastward (leeward) inclination), $v = v_0 \cos(kx + lp)$, $v_0 = \phi_0 k / f_0$, and $\partial^2 \omega / \partial x^2 = -k^2 \omega$.

Thus, equation (A.2) reduces to

$$\partial^2 \omega / \partial p^2 - \mu^2 \omega = -a^* \cos(kx + lp) - b^* \sin(kx + lp), \quad (\text{A.3})$$

where $a^* = (ak^2 v_0) / f_0^2 < 0$, $b^* = bl v_0 / f_0^2 < 0$ for $l < 0$ and $b^* > 0$ for $l > 0$, and $\mu^2 = (S_0 k^2) / f_0^2$.

The solution of equation (A.3) is

$$\begin{aligned} \omega &= \omega_1 + \omega_2 \\ &= \omega_{01} \left\{ \cos(kx + lp) + \frac{\sinh \mu p}{\sinh \mu P} [\cos kx \cosh \mu P - \cos(kx + lP)] - \cos kx \cosh \mu p \right\} \\ &\quad + \omega_{02} \left\{ \sin(kx + lp) + \frac{\sinh \mu p}{\sinh \mu P} [\sin kx \cosh \mu P - \sin(kx + lP)] - \sin kx \cosh \mu p \right\} \\ &= \omega_{01} \Omega_1(x, p) + \omega_{02} \Omega_2(x, p), \end{aligned} \quad (\text{A.4})$$

where $\omega_{01} = a^* / (l^2 + \mu^2) < 0$, $\omega_{02} = b^* / (l^2 + \mu^2) \leq 0$ for $l \leq 0$, and the upper and lower boundary conditions for ω , i.e., $\omega = 0$ at $p = 0$ and P , is used.

Using the approximate solution for ω , equation (A.4), and the assumption for ϕ , $-\partial(\omega K') / \partial p$ and its zonal mean $-\overline{\partial(\omega K') / \partial p}$ are obtained, i.e.,

$$-\frac{\partial}{\partial p} (\omega K') = -\frac{\partial}{\partial p} \left[(\omega_{01} \Omega_1 + \omega_{02} \Omega_2) \frac{v_0^2}{2} \cos^2(kx + lp) \right], \quad (\text{A.5})$$

and

$$-\overline{\frac{\partial}{\partial p} (\omega K')} = 0. \quad (\text{A.6})$$

Similarly,

$$-\omega' \phi' = -(\omega_{01} \Omega_1 + \omega_{02} \Omega_2) \phi_0 \sin(kx + lp), \quad (\text{A.7})$$

$$\begin{aligned} -\overline{\omega' \phi'} &= -\frac{\omega_{01} \phi_0}{2} \left\{ \frac{\sinh \mu p}{\sinh \mu P} [\sin lp \cosh \mu P + \sin l(P-p)] \right. \\ &\quad \left. - \sin lp \cosh \mu p \right\} - \frac{\omega_{02} \phi_0}{2} \left\{ \frac{\sinh \mu p}{\sinh \mu P} [\cos lp \cosh \mu P \right. \\ &\quad \left. - \cos l(P-p)] + 1 - \cos lp \cosh \mu p \right\}, \end{aligned} \quad (\text{A.8})$$

and

$$\begin{aligned}
 -\frac{\partial}{\partial p}(\omega'\phi') = & -\frac{\omega_{01}\phi_0}{2} \left\{ \mu \frac{\cosh \mu p}{\sinh \mu P} [\sin lp \cosh \mu P \right. \\
 & \left. + \sin l(P-p)] + l \frac{\sinh \mu p}{\sinh \mu P} [\cos lp \cosh \mu P - \cos l(P-p)] \right. \\
 & \left. - \mu \sin lp \sinh \mu p - l \cos lp \cosh \mu P \right\} \\
 -\frac{\omega_{02}\phi_0}{2} \left\{ \mu \frac{\cosh \mu p}{\sinh \mu P} [\cos lp \cosh \mu P - \cos l(P-p)] \right. \\
 & \left. - l \frac{\sinh \mu p}{\sinh \mu P} [\sin lp \cosh \mu P + \sin l(P-p)] \right. \\
 & \left. - \mu \cos lp \sinh \mu p + l \sin lp \cosh \mu P \right\}. \quad (A.9)
 \end{aligned}$$

Since $-\alpha = \partial\phi/\partial p$, $-\omega'\alpha'$ and $-\overline{\omega'\alpha'}$ turn out to be as follows:

$$-\omega'\alpha' = l(\omega_{01}\Omega_1 + \omega_{02}\Omega_2)\phi_0 \cos(kx + lp), \quad (A.10)$$

and

$$\begin{aligned}
 -\overline{\omega'\alpha'} = & \frac{l\omega_{01}\phi_0}{2} \left\{ 1 + \frac{\sinh \mu p}{\sinh \mu P} [\cos lp \cosh \mu P - \cos l(P-p)] \right. \\
 & \left. - \cos lp \cosh \mu p \right\} \\
 -\frac{l\omega_{02}\phi_0}{2} \left\{ \frac{\sinh \mu p}{\sinh \mu P} [\sin lp \cosh \mu P + \sin l(P-p)] \right. \\
 & \left. - \sin lp \cosh \mu p \right\}. \quad (A.11)
 \end{aligned}$$

Terms underlined are cancelled out when equations (A.9) and (A.11) are added to obtain the generation term of eddy kinetic energy.

APPENDIX B

COMPARISON OF NUMERICAL SOLUTIONS OF ω -EQUATION BETWEEN DIFFERENT SPACE RESOLUTIONS

In the numerical computation, the finer mesh-size, i.e., $d=200$ km. is mostly used, but for the diagnostic study, the coarser grid interval, i.e., $d=400$ km. is adopted. To see the difference between two numerical solutions of the ω -equation caused by different space resolutions, ω at points where ω has approximately the maximum absolute values is tabulated in table B.1. For the three characteristic wavelengths, $U=U(35)$, $\delta=-\frac{1}{4}$, and the realistic amplitude of the waves are used.

We notice that the difference is conspicuous for shorter waves and the maximum of difference is approximately 10 percent of the amplitude of ω .

APPENDIX C

NUMERICAL COMPUTATION PROCEDURE

Besides the vertical distribution of physical parameters such as U and S , the patterns of height field and thickness field are given at initial time. To advance the numerical prediction, the distribution of the vertical p -velocity ω is needed. In the balanced baroclinic model, the ω -equation contains the terms of reference which relate to the divergent part (χ -component) of the wind field. However, for large-scale motion, leading terms in the ω -equation are those which appear in the quasi-geostrophic model. Thus, it is assumed that the leading terms are at least one order of magnitude larger than other terms, which is treated as a forcing term, i.e.,

$$S\nabla^2\omega^{r+1} + f_0^2 \frac{\partial^2}{\partial p^2} \omega^{r+1} = F^r$$

where F^r includes the χ^r -component of the wind. Starting with a non-divergent wind which is obtained from a height field, we iterate the solving procedure of the ω -equation; first, values of the quasi-geostrophic ω are obtained, and secondly, these ω are inserted in the forcing term F through the continuity equation to get χ from the divergence. Next, again the ω -equation is solved for ω at the next cycle and so on. Here, as is pointed out by Miyakoda [18], attention must be paid to inserting the newly acquired values of ω in F in connection with the convergence. The Poisson-type equation

$$\nabla^2\chi^{r+1} + \frac{\partial}{\partial p} \omega^{*r+1} = 0$$

is solved in the present integration, where $\omega^{*r+1} = K\omega^r + (1-K)\omega^{r+1}$. As a numerical value of K , 0.5 is used.

Only at the initial time, the above-mentioned scan-cycle process is repeated until the change of ω between two cycles becomes sufficiently small. From the second time step, the χ -field at the former time level is assumed as that at the present time level and it is used as if it is the valid divergent part of the wind field.

TABLE B-1.—Values of ω (mb./hr.) for two numerical solutions of the ω -equation

Wavelength	Pressure (mb.)										
	0	100	200	300	400	500	600	700	800	900	1000
$L=12,000$ km.											
$d=200$ km.	0.00	-0.41	-0.50	-0.56	-0.60	-0.60	-0.57	-0.49	-0.37	-0.20	0.00
400 km.	0.00	-0.40	-0.50	-0.56	-0.60	-0.60	-0.56	-0.49	-0.37	-0.20	0.00
$L=6,000$ km.											
$d=200$ km.	0.00	-0.01	-0.56	-1.36	-1.78	-1.89	-1.76	-1.46	-1.05	-0.55	0.00
400 km.	0.00	-0.01	-0.54	-1.31	-1.71	-1.82	-1.69	-1.41	-1.01	-0.53	0.00
$L=3,000$ km.											
$d=200$ km.	0.00	-0.00	-0.38	-1.36	-2.15	-2.60	-2.67	-2.43	-1.90	-1.09	0.00
400 km.	0.00	-0.00	-0.35	-1.22	-1.93	-2.33	-2.39	-2.17	-1.70	-0.97	0.00

Concerning the tolerable limits of errors of the relaxation, ϵ_ω , ϵ_z , and ϵ_x , respectively, for solving the ω -equation, the vorticity equation at the lowest level and the continuity equation, the following values are used.

$$\begin{aligned}\epsilon_\omega &= 10^{-5} \text{ for } 2\Delta t \cdot \omega \text{ in unit mb. } (\Delta t: 1 \text{ hour}), \\ \epsilon_z &= 10^{-4} \text{ for } \delta t Z = 2\text{-hour height change in m.}, \\ \epsilon_x &= 10^{-3} \text{ for } \chi/d \text{ in m. mb. sec. } (d: 200 \text{ km. or } 400 \text{ km.})\end{aligned}$$

Specifically for the experiment on the effect of dissipation, ϵ is put ten times as large as the above values for the sake of saving computation time. The change of the amount of ϵ produces at the maximum a 10 percent difference in the interacting quantities. The absolute magnitude of the coupling quantities increases as the magnitude of ϵ decreases.

APPENDIX D

EXCHANGE OF THERMODYNAMICAL UNITS

In the present paper we used a unit $\text{m}^2 \text{sec}^{-3}$ for the rate of change of the kinetic energy per unit mass. If we denote it with the unit per unit volume in x, y, p coordinate system, the relation may read as follows:

$$\begin{aligned}(\) \text{ m}^2 \text{sec}^{-3} \text{ (per unit mass)} &= 88.2 \times (\) \text{ joule} \\ &\text{cm}^{-2} \text{mb}^{-1} \text{day}^{-1} \text{ (per unit volume)}.\end{aligned}$$

ACKNOWLEDGEMENTS

The research was completed during the author's stay at the National Meteorological Center (NMC), U.S. Weather Bureau, Environmental Science Services Administration (ESSA), Suitland, Md. The author wishes to express his sincere gratitude to Dr. Frederick G. Shuman, Director, NMC, for his warm hospitality and encouragement during the author's stay at NMC. The author is very grateful to Dr. Syukuro Manabe of the Geophysical Fluid Dynamics Laboratory (GFDL), ESSA, for carefully reading the original manuscript and for valuable suggestions and constructive criticisms. The author wishes to express his thanks to the following people for carefully reading the first version of the manuscript and for many helpful comments: Drs. Kikuro Miyakoda and Ernest C. Kung of GFDL, ESSA; Dr. Takio Murakami of the Meteorological Research Institute, Japan Meteorological Agency; Mr. Alvin C. Miller of the Upper Air Branch, NMC, ESSA; Dr. John B. Hovermale and Mr. William G. Collins of the Development Division, NMC, ESSA. Thanks are due to Mr. Arthur R. Kneer of the Data Automation Division and to Dr. John D. Stackpole of the Development Division, NMC, ESSA, for their useful help with the computer program. The author is much indebted to Mr. Allen E. Brinkley and Mrs. Judith A. Turner for their very helpful assistance in preparing the manuscript and the figures.

REFERENCES

1. A. Arakawa, "On the Maintenance of Zonal Mean Flow," *Papers in Meteorology and Geophysics*, vol. 8, No. 1, Apr. 1957, pp. 39-54.
2. A. Arakawa, "On the Mean Meridional Circulation in the Atmosphere," *Journal of the Meteorological Society of Japan*, The 75th Anniversary Volume, Nov. 1957.
3. A. Arakawa, "Non-Geostrophic Effects in the Baroclinic Prognostic Equations," *Proceedings of the International Symposium on Numerical Weather Prediction in Tokyo, November 7-13, 1960*, pp. 161-175.
4. B. W. Boville, "The Aleutian Stratospheric Anticyclone," *Journal of Meteorology*, vol. 17, No. 3, June 1960, pp. 329-336.
5. A. P. Burger, "Scale Consideration of Planetary Motions of the Atmosphere," *Tellus*, vol. 10, No. 2, May 1958, pp. 195-205.
6. J. G. Charney and P. G. Drazin, "Propagation of Planetary-Scale Disturbances from the Lower into the Upper Atmosphere," *Journal of Geophysical Research*, vol. 66, No. 1, Jan. 1961, pp. 83-109.
7. J. G. Charney and J. Pedlosky, "On the Trapping of Unstable Planetary Waves in the Atmosphere," *Journal of Geophysical Research*, vol. 68, No. 24, Dec. 15, 1963, pp. 6441-6442.
8. L. S. Chen, "The Vertical Propagation of Disturbances of Various Scale in the Atmosphere in a Non-Geostrophic Model," *Collected Papers on the General Circulation in the Stratosphere*, Geophysical Research Laboratories, Academia Sinica, (in Chinese; An abridged translation into Japanese by Hiroshi Ito, *Grosswetter*, vol. 3, No. 3, Jan. 1965, Longrange Forecast Group, Japan Meteorological Agency)
9. G. P. Cressman, "Barotropic Divergence and Very Long Atmospheric Waves," *Monthly Weather Review*, vol. 86, No. 8, Aug. 1958, pp. 293-297.
10. R. E. Dickinson, "Propagators of Atmospheric Motions," *Report*, No. 18, Planetary Circulation Project, Massachusetts Institute of Technology, July 1966, 244 pp.
11. A. Eliassen and E. Palm, "On the Transfer of Energy in Stationary Mountain Waves," *Geofysiske Publikasjoner*, vol. 22, No. 3, Dec. 1960, pp. 1-23.
12. E. Eliassen, "A Study of the Long Atmospheric Waves on the Basis of Zonal Harmonic Analysis," *Tellus*, vol. 10, No. 2, May 1958, pp. 206-215.
13. P. R. Julian and K. B. Labitzke, "A Study of Atmospheric Energetics During the January-February 1963 Stratospheric Warming," *Journal of the Atmospheric Sciences*, vol. 22, No. 6, Nov. 1965, pp. 597-610.
14. I. A. Kibel, "An Introduction to the Hydrodynamical Methods of Short-Period Weather Forecasting," (Translation edited by R. Baker), Pergamon Press, 1963.
15. E. C. Kung, "Kinetic Energy Generation and Dissipation in the Large-Scale Atmospheric Circulation," *Monthly Weather Review*, vol. 94, No. 2, Feb. 1966, pp. 67-82.
16. E. C. Kung, "Large-Scale Balance of Kinetic Energy in the Atmosphere," *Monthly Weather Review*, vol. 94, No. 11, Nov. 1966, pp. 627-640.
17. A. J. Miller, "Vertical Motion Atlas for the Lower Stratosphere During the IGY," *Report*, No. 16, Planetary Circulation Project, Massachusetts Institute of Technology, Jan. 1966, 35 pp. and figures.
18. K. Miyakoda, "Some Characteristic Features of Winter Circulation in the Troposphere and Lower Stratosphere," *Technical Report*, No. 14 to National Science Foundation (Grant NSF-GP-471), Dept. of Geophysical Sciences, The University of Chicago, Dec. 1963.
19. H. S. Muench, "Stratospheric Energy Processes and Associated Atmospheric Long-Wave Structure in Winter," *Environmental Research Paper*, No. 95, Air Force Cambridge Research Laboratories, Apr. 1965, 73 pp. and Appendixes.
20. H. S. Muench, "On the Dynamics of the Winter-Time Stratospheric Circulation," *Journal of the Atmospheric Sciences*, vol. 22, No. 4, July 1965, pp. 349-360.
21. T. Murakami, "Vertical Transfer of Energy Due to Stationary Disturbances Induced by Topographies and Diabatic Heat Sources and Sinks," (Unpublished Manuscript), 1966.
22. R. E. Newell, "The Circulation of the Upper Atmosphere," *Scientific American*, vol. 210, No. 3, 1964, pp. 62-74.

23. T. Nitta, "Dynamical Effect of the Variable Tropopause," *Journal of the Meteorological Society of Japan*, Series II, vol. 43, No. 2, Apr. 1965, pp. 124-137.
24. G. Onishi and H. Tanabe, "Dynamical Stability in the Stratosphere," *The Science Reports of the Tohoku University*, Fifth Series, Geophysics, vol. 17, No. 3, Mar. 1966.
25. A. H. Oort, "On the Energetics of the Mean and Eddy Circulations in the Lower Stratosphere," *Tellus*, vol. 16, No. 3, Aug. 1964, pp. 309-329.
26. L. Peng, "A Simple Numerical Experiment Concerning the General Circulation in the Lower Stratosphere," *Pure and Applied Geophysics*, vol. 61, II, 1965, pp. 191-218.
27. N. A. Phillips, "Geostrophic Motion," *Reviews of Geophysics*, vol. 1, No. 2, May 1963, pp. 123-176.
28. R. J. Reed, J. L. Wolfe, and H. Nishimoto, "A Spectral Analysis of the Energetics of the Stratospheric Sudden Warming of Early 1957," *Journal of the Atmospheric Sciences*, vol. 20, No. 4, July 1963, pp. 256-275.
29. J. Smagorinsky, S. Manabe, and J. L. Holloway, Jr., "Numerical Results from a Nine-Level General Circulation Model of the Atmosphere," *Monthly Weather Review*, vol. 93, No. 12, Dec. 1965, pp. 727-768.
30. Staff Members of Meteorology Group, Geophysics Research Laboratories, Academia Sinica, "Some Studies on the Large-Scale Weather Process," *Tenki* (in Japanese), vol. 11, No. 4, Apr. 1964, pp. 119-130.
31. S. Teweles, "Spectral Aspects of the Stratospheric Circulation During the IGY," *Report No. 8, Planetary Circulation Project*, Massachusetts Institute of Technology, Jan. 1963, 191 pp.
32. P. Welander, "Theory of Very Long Waves in a Zonal Atmospheric Flow," *Tellus*, vol. 13, No. 2, May 1961, pp. 140-155.
33. A. Wiin-Nielsen, "On Barotropic and Baroclinic Models with Special Emphasis on Ultra-Long Waves," *Monthly Weather Review*, vol. 87, No. 5, May 1959, pp. 171-183.
34. P. M. Wolff, "The Errors in Numerical Forecasts Due to Retrogression of Ultra-Long Waves," *Technical Memorandum*, Joint Numerical Weather Prediction Unit, No. 13.

[Received March 10, 1967; revised April 10, 1967]